A New Depositional Framework for Massive Iron Formations After the Great Oxidation Event

Geochemistry, Geophysics, Geosystems

RESEARCH ARTICLE
10.1029/2020GC009113

Key Points:

- Depositional settings and conditions that led to massive iron formations (IFs) are complex, yet crucial for interpreting Earth's evolution
- To determine the context and trigger for massive IF after the rise of oxygen, we combine new mapping, stratigraphic and facies data
- Dataset support syn-sedimentary faulting and IF onset tied to oxygen variations instead of shelf transgressions or syn-basinal volcanism

Supporting Information:

Supporting Information may be found in the online version of this article.

Correspondence to:

A. Eyster,
aeyster3@jhu.edu

Citation:

Eyster, A., Brengman, L. A., Nichols, C. I. O., Levitt, Z., Wilcots, J., & Bergmann, K. D. (2021). A new depositional framework for massive iron formations after the great oxidation event. *Geochemistry, Geophysics, Geosystems*, *22*, e2020GC009113. https://doi.org/10.1029/2020GC009113

Received 17 APR 2020
Accepted 14 JUL 2021

A New Depositional Framework for Massive Iron Formations After the Great Oxidation Event

Athena Eyster[1,2], Latisha A. Brengman[3], Claire I. O. Nichols[4], Zoe Levitt[1], Julia Wilcots[1], and Kristin D. Bergmann[1]

[1]Department of Earth, Atmospheric and Planetary Sciences, Massachusetts Institute of Technology, Cambridge, MA, USA, [2]Now at Morton K. Blaustein Department of Earth and Planetary Sciences, Johns Hopkins University, Baltimore, MD, USA, [3]Department of Earth and Environmental Sciences, University of Minnesota Duluth, Duluth, MN, USA, [4]Department of Earth Sciences, University of Oxford, Oxford, UK

Abstract The oldest recognized proxies for low atmospheric oxygen are massive iron-rich deposits. Following the rise of oxygen ~2.4 billion years ago (Ga), massive iron formations (IFs) largely disappear from the geologic record, only to reappear in a pulse ~1.88 Ga, which has been attributed to sea-level transgressions, changing ocean chemistry triggered by intense volcanism, or lowered atmospheric oxygen levels. The North American Gogebic Range is one of the rare records of this pulse and even more uniquely has exposures of both volcanics and IF, providing an ideal field locality to investigate triggers for this pulse of IF. To determine the environmental context and key factors driving IF deposition after the initial rise in oxygen, we made detailed observations of the stratigraphy and facies relationships and present updated mapping relationships of the Gogebic Range Ironwood Iron Formation and the Emperor Volcanics. This work expands existing mine datasets and logs to constrain variations in stratigraphy. Our results are the first to quantitatively constrain thickness variations along the entire Gogebic Range and tie them to syn-sedimentary faulting along listric normal faults and half grabens. Furthermore, our dataset suggests that initiation of intense syn-basinal volcanism linked to a large igneous province does not coincide with initial iron deposition, thus cannot be invoked as a causal trigger. Finally, the possibility of iron deposition in a shallow-water environment suggests that the post-GOE IF pulse may not reflect global marine transgressions, but instead a chemocline shallowing due to changing global atmospheric oxygen.

Plain Language Summary What can massive iron-rich rocks tell us about ancient global oxygen levels? Although these rocks have long been recognized as proxies for low oxygen, much is yet to be learned about the environments that lead to their deposition. These uncertainties are particularly apparent ~1.88 billion years ago, when, after atmospheric oxygen rose, there was a renewed peak in the appearance of iron-rich rocks. Was this iron deposition externally triggered by changing global oxygen levels or by rising inputs of volcanically sourced iron? Or does their resurgence represent internal ocean dynamics related to sea level? We present refined relationships of volcanic and iron-rich rocks in the Lake Superior region and tie variations to faulting. The data suggests that the iron deposition onset does not appear to be triggered by syn-basinal volcanism or sea-level variations, but instead may be related to atmospheric oxygen.

1. Introduction

Abundant global oxygen is crucial for macroscopic life on Earth today, yet the tempos and triggers of ancient oxygenation are unknown. Iron formations (originally defined as rocks with >15 wt. % iron; James, 1954) hold important clues to the early evolution of Earth's atmosphere and biosphere, yet questions about their genesis remain. In particular: (a) are all massive iron formations (IFs) deposited in broadly similar depositional and geochemical settings; and (b) what drives their episodic deposition? The purpose of this work is to assess these questions with a case study coupling facies-based sedimentological and stratigraphic approaches for the ~1.88 Ga Gogebic Range exposed near Lake Superior, USA (Michigan-Wisconsin), one of a few preserved post-Great Oxidation Event (GOE) massive iron deposits.

Massive IFs (~10^6 Gigatons) occur only in the Precambrian (e.g., Bekker et al., 2014; Konhauser et al., 2017). When examining the geologic record, the largest volumes of preserved IFs span the Late Archean to

Paleoproterozoic, ending rather abruptly after 1.87 Ga (Gole and Klein, 1981; Trendall, 2002; age from Fralick et al., 2002). This record could reflect continuous IF deposition that is no longer evident due to preservation bias (Johnson & Molnar, 2019), or cessation of massive IF deposition after the GOE followed by brief IF resurgence ~1.88 Ga (e.g., Bekker et al., 2014; Konhauser et al., 2017; Lyons et al., 2014).

1.1. Models for Massive Iron Formation Deposition in Shelf Environments

Stratigraphically thick, massive IFs (commonly referred to as "Superior iron formations") have been classically tied to the presence of low oxygen water masses, allowing high concentrations of dissolved ferrous iron Fe^{2+} to accumulate, and the global dynamics of broad, stable, continental shelf environments (Bekker et al., 2014; Gross, 1983; Klein, 2005). Low atmospheric and dissolved oxygen conditions are only two of several requirements for massive iron deposition (see Konhauser et al., 2017 for a thorough review). First, anoxic water conditions (<1 mM dissolved oxygen) are required for ferrous iron (Fe^{2+}) to accumulate. There also must be a Fe^{2+} source either from weathered continental material or hydrothermal/magmatic material introduced directly into the water column. These prerequisites are crucial for accumulating massive volumes of iron. Finally, the dissolved iron must precipitate out of solution in order to be deposited as sediment. This can happen through oxidation of Fe^{2+} to Fe^{3+} (the classically proposed model) or direct precipitation of iron silicates or green rust (e.g., Halevy et al., 2017; Johnson et al., 2018; Rasmussen et al., 2016; Tosca et al., 2016). Differentiating between these specific chemical processes is complicated by incomplete geologic preservation and transformation of primary iron mineralogy to secondary iron-carbonates, iron-silicates, or iron oxides (e.g., Rasmussen et al., 2016; Robbins et al., 2019).

Within this framework, IF deposition on shelves has commonly been interpreted as reflecting major transgressive events (Beukes, 1983; Ojakangas, 1983) and limited clastic delivery (Fralick & Barrett, 1995), and not necessarily dramatic variations in ferrous iron concentrations. These massive IF deposition models are consistent with extensive Archean and Paleoproterozoic deposits found in Australia and South Africa. There, the IF sedimentology, sequence stratigraphy, proximal platformal carbonate associations, and asymmetrical occurrence of IFs across the platform margins support deep-water, sediment-starved facies interpretations (e.g., Beukes, 1983; Fischer & Knoll, 2009; Klein & Beukes, 1992a, 1992b; Knoll & Beukes, 2009; Morris & Horwitz, 1983). These deposits are predominantly banded IFs, interpreted to be chemical muds with well-developed, thin, primary laminations and bedding with alternating iron-rich and iron-poor layers, the iron poor-layers being dominantly chert (e.g., Gross, 1983; Knoll & Beukes, 2009; Simonson, 2003).

Although massive IFs were deposited both before and after the GOE, they display sedimentological variations across this important atmospheric change. After the GOE, massive IFs were deposited ~1.88 Ga, predominantly around Lake Superior (North America) (Bekker et al., 2014; Konhauser et al., 2017; Simonson, 2003). These younger deposits possess distinct textures and are primarily composed of "granule" clasts that range in size from fine to coarse sand and are well-rounded to angular (e.g., Mengel, 1973; Simonson, 2003; Van Hise & Leith, 1911) instead of being dominantly banded. Early work on these post-GOE IFs suggested that they were stable transgressive shelf deposits due to: (a) their size and extent (e.g., Kimberley, 1989), (b) the lack of evidence for subaerial exposures (e.g., Ojakangas, 1983), (c) the lack of chemical and mineralogical variability expected from closed basins (e.g., Gole & Klein, 1981; Lepp, 1987), and (d) their conformable position within a transgressive sequence between subtidal quartzites and slope shales (e.g., Ojakangas, 1983; Simonson & Hassler, 1996).

More recently, geochronological data (Addison et al., 2005) and identification of subaerial exposure surfaces in key sequences (Fralick et al., 2017) have demonstrated that slope shales may be separated in time from iron deposition. Furthermore, documentation of cross-stratification has been used by some authors to suggest that the granular IF may represent shallow-water deposits (Simonson, 1985, 2003), although others argue these may reflect deeper water storm deposits (Pufahl & Fralick, 2004). Finally, as it is equivocal if all the post-GOE IFs that surround the Lake Superior region were deposited in the same basin (e.g., Konhauser et al., 2017; Morey & Southwick, 1995; Ojakangas et al., 2001; Pufahl & Fralick, 2000), geologic observations from one sequence may not be directly applied to others without independent verification and proof. Therefore, it is still uncertain if all massive IFs, and in particular the post-GOE massive IFs, fit a transgressive systems tract depositional model.

Furthermore, the driver of IF deposition is still unknown. The post-GOE IF pulse may simply reflect a global sea-level transgression. Alternatively, IF deposition could be triggered by variation in the physical environment (e.g., a change in atmospheric oxygen, tectonic or magmatic events; Bekker, et al., 2014). Indeed, the post-GOE IF pulse has been attributed to three different competing hypotheses: (a) sea-level rise, (b) intense volcanism, and (c) fluctuating atmospheric oxygen, basin chemistry or pH (e.g., Barley et al., 2005; Bekker et al., 2010; Ernst & Bell, 2010; Rasmussen et al., 2012; Simonson & Hassler, 1996). Understanding both the depositional and tectonic framework of post-GOE IF deposits is crucial for interpreting their global significance and distinguishing between these various models.

A key variable is the link between iron deposition and active volcanism which has been suggested as both an iron source and a depositional trigger (e.g., Derry & Jacobsen, 1990; Huston & Logan, 2004; Isley & Abbott, 1999). We place particular interest on the more recent hypothesis that an increase in igneous activity triggered the pulse via a large addition of Fe^{2+} into the oceans, allowing a switch to ferruginous conditions and iron deposition (e.g., Fralick et al., 2017; Rasmussen et al., 2012). This shift in igneous activity could have been tied to large igneous province development related to a mantle plume, rift-extensional magmatism tied to supercontinent dynamics, accretionary magmatism related to a pulse of orogenesis, or enhanced mid-ocean ridge spreading (e.g., Fralick et al., 2017; Huston & Logan, 2004; Isley & Abbott, 1999; Konhauser et al., 2017; Rasmussen et al., 2012). Geologic evidence supports a ~1.88 Ga Circum-Superior magmatic province, which bolsters the possibility of a genetic link that large scale volcanism triggered iron deposition (Bleeker & Kamo, 2017; Conliffe, 2015; Konhauser et al., 2017). A complicating factor is that many of the preserved volcanics tied to this "global pulse" also outcrop across the Superior craton in close association with the IFs themselves, suggesting that the global pulse may have manifested itself as syn-basinal volcanism that influenced IF deposition. Detailed work to better identify the conditions for iron deposition onset and the relationships to eruptive volcanism can help to detangle causal mechanisms.

To address uncertainties in the depositional and tectonic context and key factors driving deposition of these post-GOE IFs we focus on representative post-GOE strata from the North American Gogebic Range in the Lake Superior region (Figures 1a–1c), one of seven major deposits that represent the bulk of post-GOE IFs (e.g., Bekker et al., 2014). This locality was chosen as a target as easily accessible outcrops of both volcanics and IF have been suggested to be consistent with both the transgression triggered iron deposition (e.g., Ojakangas, 1983) and volcanically triggered iron deposition (e.g., Cannon et al., 2008; Sims et al., 1984). The Gogebic Range is of particular interest as the associated volcanics have been tied to the Circum-Superior Magmatic Province (Ciborowski et al., 2017; Minifie et al., 2013). If these syn-basinal volcanics are consistently found stratigraphically beneath the IF, this would provide compelling evidence for syn-basinal Circum-Superior Province volcanism as a trigger for the onset of post-GOE IF. To clarify syn-basinal and regional relationships between tectonic, volcanic activity and IF deposition as well as test the transgressive shelf model for IFs deposited after the GOE such as in the Gogebic Range, we make new stratigraphic observations and present updated mapping relationships. We combine our field observations with other datasets to construct a sedimentologic and volcanic facies framework, identify variations in stratigraphy and elucidate the depositional context for the onset of IF.

1.2. Geologic Context

Broadly correlative, post-GOE IF deposits are found across the Lake Superior region, as well as localities in Northeast Canada and Western Australia (Figure 1a, also see Rasmussen et al., 2012 and references therein). The proposed depositional environments of these IFs are not uniformly agreed upon. Across the Lake Superior region potentially correlative IF basins are thought to reflect dynamics on the present-day southeast margin of the Superior craton (Figure 1b). These include the Gogebic Range of northern Michigan (Hotchkiss, 1919; Pufahl & Fralick, 2004), the Negaunee and Riverton Iron Formations of northern Michigan (James, 1954, 1955); the Mesabi Range (Biwabik Formation) and poorly studied Cuyuna Range in Minnesota (French, 1968, 1973) and the Gunflint Iron Formation in Ontario, Canada (Floran & Papike, 1975). More globally, potentially correlative IFs are found farther north in the Labrador Trough of Canada, the Sokoman Iron Formation (Gross & Zajac, 1983; Klein, 1966, 1973, 1978, 1983; Klein & Fink, 1976; Zajac, 1974) and in the Earaheedy/Nabberu Basin of Western Australia, Frere Iron formation (Bunting, 1986; Goode et al., 1983; Hall & Goode, 1978; Rasmussen et al., 2012).

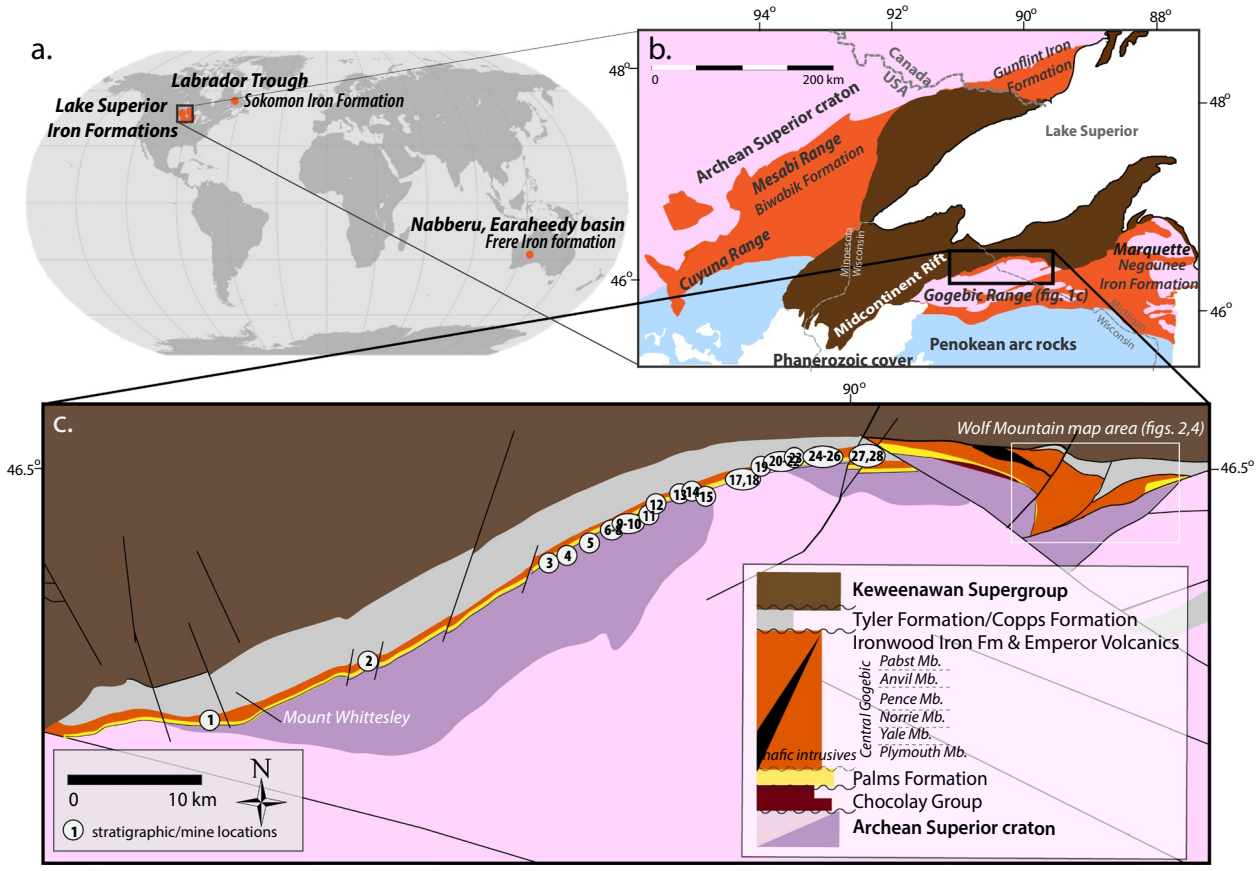

Figure 1. (a) Global outcrops of ~1.88 Ga Iron formations. (b) Map depicting the sequences around Lake Superior (after Reed & Daniels, 1987; Schulz & Cannon, 2007; Sims, 1992). The Gogebic Range is highlighted by the thick box. (c) Gogebic Range geologic map. Numbers indicate locations of stratigraphic sections in Figure 6: (1) West side of Penokee Gap; (2) Tyler's fork; (3) Atlantic; (4) Plumer Shaft; (5) Pence; (6–8) Montreal; (9, 10) Ottawa; (11) Cary; (12) Windsor; (13) Ashland; (14) Norrie; (15) Aurora; (17) Davis; (18) Geneva; (19) Puritan; (20) Ironton; (21) Ironton; (22) Yale; (23) Colby; (24–26) Tilden; (27) Eureka; (28) Mikado. Inset depicts the schematic stratigraphy of the Gogebic Range.

Among these various basins, we chose to focus on the Gogebic basin as it has been cited as an ideal case study to test these competing hypotheses. The Gogebic Range extends from Lake Gogebic in Michigan, westward ~128 km into Wisconsin (Figure 1c). The focus of this work is a sequence of mixed carbonate and siliciclastic rocks, IF, and volcanics that unconformably and variably overlies Archean basement rocks and early Paleoproterozoic strata (Aldrich, 1929; Allen & Barrett, 1915; Cannon et al., 2008; Hotchkiss, 1919; LaBerge, 1964; Laybourn, 1979; Prinz, 1981; Schmidt, 1980; Van Hise & Lieth, 1911 for more details).

The general stratigraphy in the Gogebic Range, with basal sandstones, followed by IF and capped by shales, has long been recognized as being similar to the Sokoman, Biwabik, Gunflint, and Negaunee Iron Formations. However, it has since become apparent that unconformities exist between the IF and the overlying shales in many of these ranges. Furthermore, work in the Sokoman Iron Formation suggests that there may also be a basal unconformity (Pufahl et al., 2014). Regardless of these details, the broad similarity of the Gogebic Range stratigraphy with the other iron deposits highlights its utility in clarifying basin dynamics involved in massive iron deposits.

Iron formation in the Gogebic Range overlies the Palms Formation, a sequence of basal mudstone-siltstone, middle interbedded mudstone-siltstone-sandstone, and upper sandstone. Early interpretations suggested that the basal Palms Formation represented a transgressive sequence in a tidal-subtidal shelf setting, and the overlying Ironwood Iron Formation represented a continuation of the transgressive sequence as the time-equivalent deeper water correlative to the Palms Formation (e.g., Ojakangas, 1983). More recent interpretations suggest that the Ironwood Iron Formation was deposited on a southward sloping continental shelf (Pufahl & Fralick, 2004). Currently, this basin has been variably described as either a foreland basin

(Hoffman, 1987; Klasner et al., 1991; Southwick & Morey, 1991), or an extensional basin on the edge of the craton, such as a back-arc basin (Fralick et al., 2002; Hemming et al., 1995; Schulz & Cannon, 2007; Van Wyck & Johnson, 1997).

In the central part of the range, the Ironwood Iron Formation itself has been divided into five members (Figure 1): the Plymouth, Yale, Norrie, Pence, and Anvil members (e.g., Cannon et al., 2008; Hotchkiss, 1919; Schmidt, 1980). These Ironwood Iron Formation members have been difficult to distinguish on the eastern portion of the Gogebic Range, in part due to the Emperor Volcanics near Wolf Mountain, Michigan (Cannon et al., 2008; Dann, 1978; Irving & Van Hise, 1892; Sims et al., 1984; Trent, 1973). The Emperor Volcanics range from basaltic to dacitic compositions and have been metamorphosed to lower greenschist facies.

Variably overlying the Ironwood Iron Formation and Emperor Volcanics are immature siliciclastic rocks of the Tyler Formation (western range) and Copps Formation (eastern range), which have previously been suggested to be deposited in a foredeep (foreland) basin associated with Penokean collision (see Ojakangas et al., 2001; Schulz & Cannon, 2007; Van Wyck & Johnson, 1997 for more details). Although outside the direct scope of this study, this tectonic setting may conflict with existing datasets (e.g., Addison et al., 2005; Morey, 1969; Poulton et al., 2010; Sims et al., 1989), and its evolution is contentious (Zi et al., 2021). Such convergent deformation and regional metamorphism are not temporally unique to this region. The Superior, Nain, and Slave cratons collided to form the supercontinent Nuna ~1.6 Ga and which was tied to juvenile crust accretion at the margins (e.g., Bleeker, 2003; Evans & Mitchell, 2011; Evans et al., 2016; Hoffman, 1988).

After the Penokean orogeny, the region experienced erosion followed by the eruption and deposition of the younger Keweenawan Supergroup associated with the ca. 1.1 Ga Mesoproterozoic Midcontinent Rift system (e.g., Davis & Paces, 1990). About 30 million years after rifting, the Grenville orogeny to the east placed the region under compression, causing normal faults to be reactivated as reverse faults (Cannon, 1994).

2. Methods

2.1. Classification of Iron Facies

A facies table (Table 1) was constructed based on observations from outcrops and exposures surrounding Wolf Mountain combined with observations from Mount Whittlesey and published field and mine observations from along the Gogebic Range (Hotchkiss, 1919; Laybourn, 1979; Schmidt, 1980). In the Wolf Mountain locality, individual outcrops and test pits were identified via field transects and published outcrop locations (Klasner et al., 1998; Trent, 1973). At each outcrop, variations in textures, structures, bedforms, grain size and any contact relationships were recorded. Many early researchers utilized "cherty" versus "slaty", "wavy" versus "parallel" terminology to describe the Ironwood Iron Formation (e.g., Huber, 1959; LaBerge, 1964). Such terminology employed "cherty" IF to refer to sand-sized chert and iron mineral grains within a chert matrix, and "slaty" IF to involve laminated silt-sized chert and iron mineral grains. However, more recent work has identified the inappropriateness of this classification scheme for sedimentological investigations (Simonson, 1985). Thus, we used terms such as conglomerate (grains >2 mm), grainstone (grains 0.0625–2 mm), and mudstone (grains <0.063 mm). We also avoided the term "wavy" unless referring to the specific depositional sedimentary structure. Finally, we chose to combine iron-carbonates, iron-oxides, and iron-silicates under the classification of "iron minerals." While there is important primary and diagenetic information in the distribution of iron minerals across the Gogebic Range, we made this decision to sidestep the debate regarding their original mineralogy (e.g., Johnson et al., 2018; Rasmussen et al., 2016, 2019; Robbins et al., 2019), and encompass the current mineralogical heterogeneity while maintaining focus on the stratigraphic and sedimentological details.

2.2. Classification of Volcanic Facies

Volcanics were described following standard terminology using descriptive terms and a facies approach (Cas & Wright, 1987; McPhie et al., 1993). Because of the diverse genetic processes involved in the formation of volcanic deposits, two descriptive categories were used, "volcaniclastic" or "coherent" (McPhie et al., 1993). Volcaniclastic particles may be any shape or size and no specific clast forming processes, or

Table 1
Sedimentary Iron Facies Table

Facies	Description	Interpretation
Symbol. name	Lithology/composition, grain size, texture, structures/jointing/bedding	Facies association, depositional environment, and formation-member occurrence
IF1. Ferruginous grainstone	Grainstone with iron-rich coating on quartz and chert grains, chert cement & fine chert lenses. bi-directional/flaser cross bedding and fine iron mudstone laminations. Rounded medium-coarse quartz grains, chert and lithic fragments.	Facies Assoc.: Underlies IF2 and IF4, IF10 tends to be at base Dep. Env.: Moderate to high energy, intertidal-subtidal or foreshore-shoreface beach Alt. 1: lower shoreface-shelf transition zone with strong iron mudstone input Formations/members: Ironwood Iron Formation undiff. and Plymouth member
IF2. Iron grainstone	Moderately well-sorted with medium-coarse iron-mineral and chert grains. Some chert grains are coated. Can include mudstone drapes and massive to cross-bedded lenses. Occasional graded beds or intraclasts (1–3 cm in length) of IF4 or IF6 at bed bases. Subunit IFN2A – Iron-chert grainstone with iron- mudstone interbeds. Moderately well-sorted with medium-coarse iron-mineral and chert grains comprising lenses.	Facies Assoc.: Laterally equivalent to VF4, interbedded with VF3 Dep. Env.: Moderate-high energy intertidal-subtidal shoals or foreshore-shoreface, Alt. 1: storm influenced inner-mid shelf Formations/members: Ironwood Iron Formation undiff. & Plymouth, Norrie, Anvil Mbrs.
IF3. Iron-chert conglomeratic grainstone	Subunit IF3A—Chert-iron grainstone with lenses and layers of chert- grainstone with interbedded lenses dominated by pebble clasts. Subunit IF3B—Iron-chert rip-up intraformational conglomerate with angular fragments of green-gray chert and angular laminated clasts in a granular chert-iron matrix. Clast supported.	Facies Assoc.: IF3B-IF3A are gradational and associated with IF2 Dep. Env.: High energy Intertidal-subtidal or foreshore-shoreface storm deposits. Alt.: Gravely lag deposits on mid-shelf Formations/members: Ironwood Iron Formation undiff. & Plymouth, Norrie, Pence, Anvil Mbrs.
IF4. Thin-bedded iron mudstone	Uniform thin-bedded (mm-cm) and parallel laminated iron formation comprised of fine well-sorted iron-minerals (<0.1 mm). Some interbedded thin microcrystalline chert beds (some internally graded). Subunit IF4A—Green thin-bedded iron mudstone, distinguishable greenish color. Subunit IF4B. Convolute bedded iron mudstone sometimes with interbeds composed entirely of iron mudstone intraclasts.	Facies Assoc.: Interbedded with IF2 and VF1, underlies VF4, laterally equivalent to IF6, IF2. Dep. Env.: Low energy subtidal muds or lower shoreface-offshore, Alt. 1: supratidal-intertidal flats, Alt. 2: mid shelf; IF4B: Slumps formed during earthquake-induced subsidence, Alt. 1: intertidal-subtidal channel lag deposit, Alt. 2: tidal flat storm deposit Formations/members: Ironwood Iron Formation undiff. & Plymouth, Yale, Pence, Anvil Mbrs.
IF5. Thin-bedded iron mudstone-chert grainstone	Thin-bedded iron mudstone comprised of very fine sand to silt iron-minerals. Interbedded with lenses and lag deposits 3–10 cm thick of medium to very fine chert- iron grainstone. A few chert- grainstone and pebble lenses. May contain chert interbeds.	[a]Facies Assoc.: VF1, laterally equivalent with IF9 and IF8 Dep. Env.: Low-moderate energy intertidal flat, Alt. 1: shoreface-shelf transition, Alt. 2: Mid-outer shelf Formations/members: Ironwood Iron formation-Yale Member, Emperor Volcanics-member A
IF6. Thin-bedded chert	Thin-medium-bedded (1–30 cm beds) gray-greenish gray-yellow microcrystalline chert. Hematite staining can turn it red. Subunit IF6A—Thin-bedded chert with dispersed interbeds of iron mudstones or ferruginous siltstone. Subunit IF6B—Thin-bedded chert and iron grainstone—interbedded chert-iron grainstone lenses.	[a]Facies Assoc.: Laterally equivalent to IF4 Dep. Env.: Low energy supratidal-intertidal, Alt.: mid-outer shelf, Alt. IF6A: low-moderate energy Intertidal/lagoonal, Alt. IF6B: moderate energy shoreface-foreshore Formations/members: Ironwood Iron formation-Plymouth, Pence Mbrs.

Table 1
Continued

Facies	Description	Interpretation
Symbol. name	Lithology/composition, grain size, texture, structures/jointing/bedding	Facies association, depositional environment, and formation-member occurrence
IF7. Iron conglomerate	Angular-rounded cobbles of laminated chert, iron mudstone, and chert grainstone. Highly variable and poorly sorted. Subunit IF7A—Sub-rounded to round quartz cobbles supported in a tan/brown iron grainstone matrix. Beds are 20–30 cm. Subunit IF7B—Moderate-very poorly-sorted clasts supported by massively bedded matrix composed of fine iron grainstone to iron mudstone, occasional siliciclastic component. Pebble -boulder clasts include bedded quartzite and laminated hematite-rich chert (IF6).	Facies Assoc.: IF7A underlies VF4. IF7B associated with VF1. Dep. Env.: High energy fault influenced deposition, Alt. 1: Backshore , Alt. 2: Debris flows Formations/members: Ironwood Iron Formation undiff. and Pabst Member
IF8. Gray massive clastic unit	Dull gray massive beds. Some containing well-sorted black-gray rounded to angular fragments up to 4 mm.	[a]Facies Assoc.: Laterally equivalent with IF5, IF9 Dep. Env.: Volcanically influenced sedimentation Formations/members: Ironwood Iron formation-Yale Member
IF9. Black laminated iron mudstone	Dark gray-black partly pyritic, possibly argillaceous with no chert layers. Very finely laminated with disseminated black carbon.	[a]Facies Assoc.: Laterally equivalent with IF5 and IF8 Dep. Env.: Low energy upper tidal flat, Alt.: offshore mid-outer shelf Formations/members: Ironwood Iron formation-Yale Member
IF10. Stromatolite Conglomerate	Irregular stromatolites (2–10 cm high, 1–3 cm diameter) composed of chert and hematite with fine laminae. Includes fine-medium chert/iron-mineral grains with scattered quartz.	[a]Facies Assoc: Associated with IF1 and IF4A in central Gogebic Range. Dep. Env.: Low-moderate energy intertidal-subtidal, Alt.: subtidal-inner shelf reef Formations/members: Ironwood Iron formation-Plymouth Member

[a]Specifically from stratigraphic descriptions by Hotchkiss (1919); Schmidt (1980); Pufahl and Fralick (2004); and, in some cases, exposures at Mount Whittlesey.

settings are implied (autoclastic, pyroclastic, resedimented: volcanic clasts and syn-eruptive resedimentation, and volcanogenetic sedimentary: clasts both volcanic and sedimentary and sedimentation due to post-eruptive reworking). Coherent deposits occur principally from effusive lava flows and intrusions from cooling and solidification of molten lava/magma. In particular, the composition, textures, and flow and joint structures for coherent lavas and intrusions, and grain size, component compositions and textures, and bedding structures for volcaniclastic deposits were recorded (Table 2). Then, facies associations were created in order to group volcanics into genetic classifications and likely eruptive phases.

2.3. Stratigraphic Thicknesses Across the Gogebic Range

Our refined geologic mapping in the Wolf Mountain area, including recognition of facies relationships and marker horizons, allowed fault block geometry to be refined and new named faults to be identified. Stratigraphic thicknesses were measured perpendicular to strikes and corrections for local dips were applied within each interpreted fault block. Area stratigraphic thicknesses were also corrected for any later mafic intrusions into the sections. To obtain robust stratigraphic thicknesses across the Gogebic Range, we compiled published mine sections and logs from the western Penokee gap to the eastern Mikado mine (see Table S2 for location information [Hotchkiss, 1919; Schmidt, 1980]). These sections were combined with new estimated thicknesses from our refined geologic mapping of the Wolf Mountain area to construct a fence diagram along strike of the entire Gogebic Range.

Table 2
Volcanic and Siliciclastic Facies Table

Facies	Description	Interpretation
Symbol. name	Lithology/composition, grain size, texture, structures/jointing/bedding	Facies association, depositional environment, and formation-member occurrence
VF1. Massive basalt	Coherent flows (30 cm–3 m thick) of tan-gray basalt. Generally non-vesicular and aphanitic although some contain plagioclase phenocrysts.	Facies Assoc.: IF4 and IF7 Dep. Env.: Subaqueous effusive eruptions and sheet flows (lack of pillows may indicate proximal environments). Formations/members: Ironwood Iron Formation
VF2. Pillow basalt	Coherent, purple-brown colored basaltic andesite flows that weather brown. Pillows are generally aphanitic, do not have abundant vesicles, and display tortoise shell contraction cracks.	Facies Assoc.: Above IF4, IF5, IF7, below VF4 Dep. Env.: Subaqueous effusive eruptions Formations/members: Ironwood Iron Formation
VF3. Black basaltic-andesitic volcaniclastic sandstone and breccia	Volcaniclastic basaltic andesite that is black fresh and weathers tan-beige. Subunit VF3A—Coarse poorly sorted volcaniclastic basaltic andesite. Cobble-to-sand-sized clasts consist of orange-brown crystal and volcanic lithic fragments and altered glass range in size. Certain clasts appear to be "pseudo fiame." Generally matrix-supported by fine grained matrix with plagioclase laths. Subunit VF3B—Fine sand basaltic-andesitic volcaniclastic sandstone. Well-sorted, parallel to cross-bedded, isolated sub-angular jasper clasts.	Facies Assoc.: Overlies-laterally equivalent to IF2 and underlies VF4 & VF5 Dep. Env.: Explosive mass flow deposit Formations/members: Emperor Volcanics-member A
VF4. Basaltic-andesitic volcaniclastic breccia	Volcaniclastic basaltic andesite that is green-purple color when fresh, and pale beige-brown weathered. Clast supported by cobble to sand-sized angular volcanic clasts in a matrix of the same composition, and generally poorly sorted and massively bedded. Clasts display pale-white margins, jig-saw fits, and curvi-planar surfaces. Well-sorted sand- sized lenses and beds throughout, including armored lapilli.	Facies Assoc.: IF5 and overlies VF3B Dep. Env.: Explosive hyaloclastite deposit Formations/members: Emperor Volcanics-member A
VF5. Dacitic-andesitic volcaniclastic breccia	Volcaniclastic andesite that is pale green-gray when fresh, and weathers white-tan. Clast supported by sand-cobble subangular-subrounded volcanic clasts in a matrix of the same composition. Some clasts are curviplanar and display quenched rims. The thick beds are poorly sorted and massive. Some beds appear to be reverse graded. Finer volcaniclastic unit with intermediate composition matrix and sand to gravel mafic clasts commonly at base.	Facies Assoc.: overlies deposits of VF3-4, associated with VF6 and underlies VF7-VF8 Dep. Env.: Subaqueous hyaloclastite and epiclastite at base Formations/members: Emperor Volcanics-member B
VF6. Dacitic-andesite flow	Coherent pale green-gray fresh andesite flows that weather gray-pale tan. Generally aphanitic with fine plagioclase and amphibole crystals. Abundant vesicles aligned with flow banding and filled in with quartz and calcite. Discontinuous lenses.	Facies Assoc.: Associated with VF5 (as fine lenses), more abundant up section Dep. Env.: No specific indicators, but VF5 associations likely subaqueous Formations/members: Emperor Volcanics-member B
VF7. Amygdaloidal basaltic breccia	Coherent purple-brown autoclastic basalt-breccia weathers brown. Aphanitic but contains abundant vesicles (now filled with quartz and calcite). Breccia is clast supported by angular cobble sized clasts with pale-white margins. Displays jigsaw fit. Flows appear massive.	Facies Assoc.: Associated with VF8/overlying VF4/underlying VF9-VF10 Dep. Env.: Subaqueous hyaloclastite breccia Formations/members: Emperor Volcanics-member C

Table 2
Continued

Facies	Description	Interpretation
Symbol. name	Lithology/composition, grain size, texture, structures/jointing/bedding	Facies association, depositional environment, and formation-member occurrence
VF8. Dacitic-basaltic volcaniclastic breccia with mafic matrix	Volcaniclastic clast supported unit with cobble-pebble pale green-tan angular to subangular volcanic clasts in a mafic black-green matrix.	Facies Assoc.: Generally underlying VF9-10 & overlying VF5-6 Dep. Env.: Re-sedimented mass flow deposits Formations/members: Emperor Volcanics-member C
VF9. Pillow-breccia basalt	Coherent-autoclastic basalt. Black-green weathering and dark-gray fresh aphanitic basalts. Abundant epidote and quartz veins. Clast supported by cobble angular volcanic clasts displaying jigsaw fits and faint quenched rims. Some clasts display pillow morphologies.	Facies Assoc.: Associated with VF10 Dep. Env.: Subaqueous hyaloclastite-pillow breccia Formations/members: Emperor Volcanics-member D
VF10. Dark basalt flow	Coherent-autoclastic dark black-green, aphanitic basalt. Some units are amygdaloidal and contain jasper clasts/interbeds.	Facies Assoc.: Associated with VF9 and overlies IF5 Dep. Env.: No specific indicators, but lateral VF9 associations likely subaqueous Formations/members: Emperor Volcanics-member D
SF1. Shale	Well-sorted tan fine mudstone with parallel laminations.	Facies Assoc.: Unconformably overlying basement and gradationally underlying SF2. Dep. Env.: Low energy supratidal- intertidal flats Formations/members: Palms Formation
SF2. Shale-siltstone-sandstone	Medium- to well-sorted mud-medium grains composing tan fine mudstone-sandstone. Displays flaser crossbeds and mudstone partings with sandstone lenses.	Facies Assoc.: Gradationally overlying SF1 and underlying SF2 Dep. Env.: Low-moderate energy intertidal flats Formations/members: Palms Formation
SF3. Mature sandstone	Sub rounded medium sized well-sorted tan-beige mature sandstone. Parallel and cross bedded.	Facies Assoc.: Gradationally overlying SF2 Dep. Env.: Moderate-high energy intertidal-subtidal or foreshore- shoreface beach Formations/members: Palms Formation
SF4. Immature siltstone-sandstone	Chemically and texturally immature gray weathering poorly-sorted siltstone-sandstone composed of mud, quartz, lithics, plagioclase feldspar. Massively bedded. Graded beds described.	Facies Assoc.: Unconformably overlies VF9, VF10, IF5 and IF2 Dep. Env.: Slope-shelf turbidites Formations/members: Copps Formation

3. Data and Interpretations

3.1. Facies Descriptions

3.1.1. Facies Descriptions of Iron Formation

In Wolf Mountain, there are IF outcrops in the north and central portions of the map area, along with scattered test pits (Figure 2). To the west, partial sections are exposed, such as at Mount Whittlesey. As the most complete sections of the Gogebic Range IFs were obtained from mining company test drill holes and now inaccessible mines, it is difficult to reinterpret the facies descriptions and interpretations without new first-hand observations. We attempt to provide a reanalysis using a new facies framework but refer readers to Hotchkiss (1919) and Schmidt (1980) and references therein for original descriptions. The facies are described here and elaborated on in Table 1 and in the Text S1 and S2. Broadly the IF facies (Figure 3a)

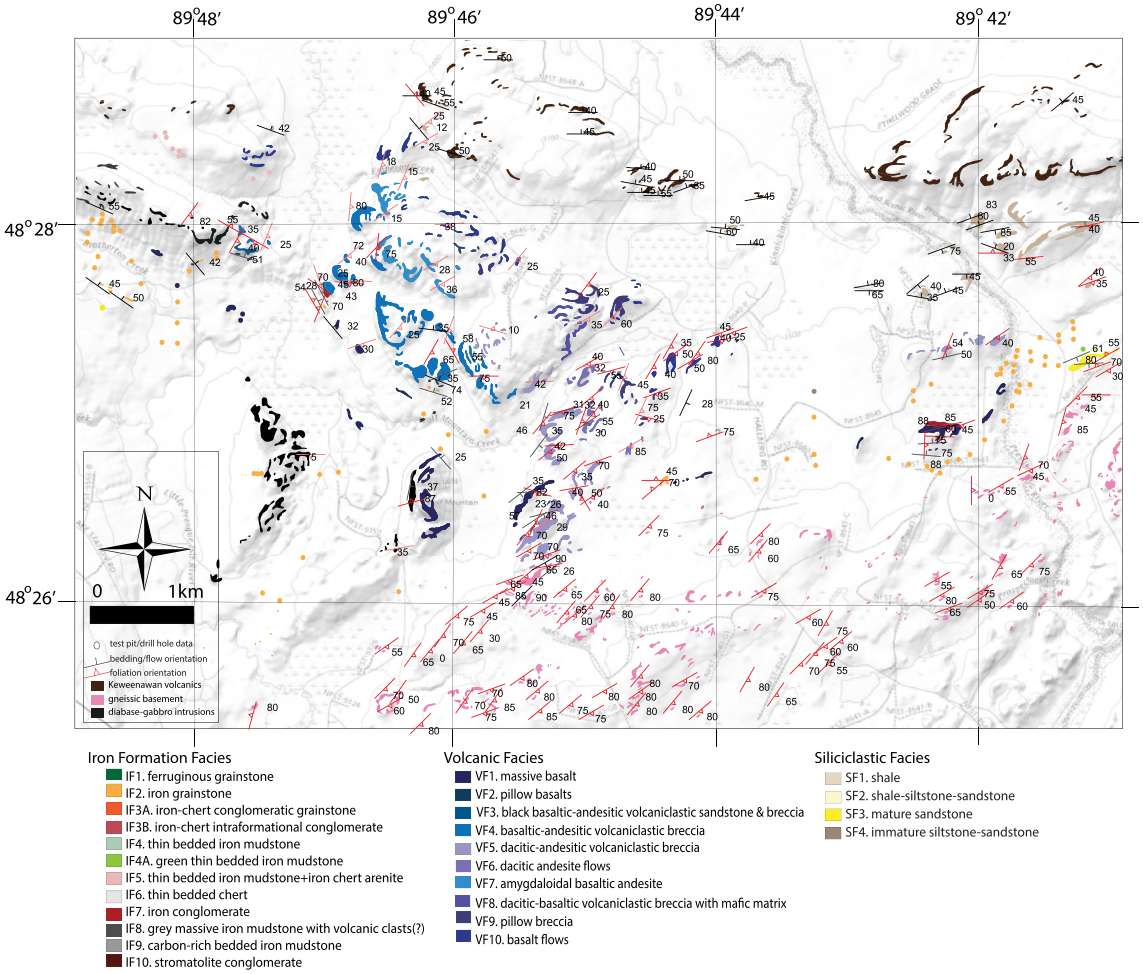

Figure 2. Wolf Mountain outcrop map with new facies classifications. For Wolf Mountain location, see Figure 1c. Dots indicate locations of test pits and data from older mining drill holes. Their lithologies are based on direct test-pit and reported drill hole observations (e.g., Klasner et al., 1998; Prinz, 1967; Trent, 1973). Interpretations of this outcrop map are shown in Figure 4.

fall into three categories, iron grainstones (facies IF1, IF2, IF3), iron mudstones (facies IF4, IF5), and iron conglomerates (IF7).

In the Wolf Mountain area, ferruginous grainstone facies IF1 is the stratigraphically lowest exposure of the Ironwood Iron Formation and displays bi-directional and uni-directional flaser cross-laminations with fine iron mudstone partings (Figure 3a i, ii). Although the contact is covered by dirt, it appears to abruptly change to facies IF2. Facies IF2 (Figure 3a iii) is completely dominated by iron and chert mineralogy and includes similar cross-bedded lenses. This unit is likely similar to the “wavy cherty granular IF” (Hotchkiss, 1919) or "upper cherty" previously described (Pufahl & Fralick, 2004). After a 5 m covered interval, outcrops of IF4 (Figure 3a iv) are documented including likely laterally equivalent subcrop displaying bright green iron mudstone, similar to IF4A. The iron mudstone IF4 in the Wolf Mountain area is similar to descriptions of a basal “parallel slaty IF” across the Gogebic Range (Hotchkiss, 1919; Pufahl & Fralick, 2004) and IF4A is similar to the "footwall slate" (e.g., Hotchkiss, 1919; Schmidt, 1980).

Continuing up-section, much of the unit is covered except for isolated test pits where facies IF2 (with possibly some beds of IF5) is documented. In the northwestern Wolf Mountain area, there are test pits displaying IF5, a thin-bedded iron mudstone-chert grainstone, that is similar to IF4, but contains chert-iron grainstone lenses. Facies IF5 is likely described previously across the range as “parallel-wavy laminated lower slaty with minor ripple cherty units” (Pufahl & Fralick, 2004).

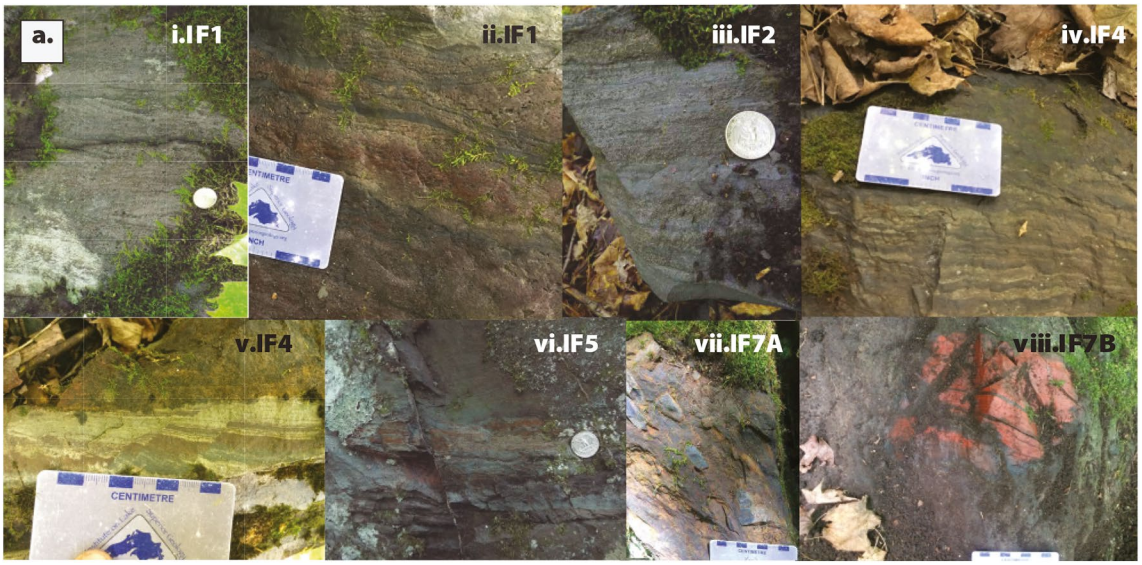

Figure 3. Field Photos. (a) Iron formation facies: (i, ii) flaser and cross-bedded structures in IF1. (iii) iron grainstone of IF2 (iv), basal iron mudstone of IF4, (v) syn-sedimentary microfaults in iron mudstone (IF4) below contact with basal Emperor Volcanics, (vi) mixed iron mudstone-grainstone (IF5) associated with VF1, (vii) iron conglomerate with quartz clasts (IF7) below contact with basal Emperor Volcanics, (viii) iron conglomerate (IF7) with clasts of IF6 that was overlying VF1 halfway up iron formation stratigraphy. Note: IF8-10 were not documented in the Wolf Mountain map area.

In the Wolf Mountain area, this lack of exposure generally continues until the upper contact with the volcanic facies VF3, VF4, or VF5 is approached. However, about halfway toward this contact, massive basalt flows (VF1) are found in association with upper IF outcrops of facies IF4 (Figure 3a v), IF5 (Figure 3a vi), and IF7 (Figure 3a vii). This initial effusive basaltic volcanism (VF1) is not found to directly underlie IF facies, but instead occurs near the upper contact between the iron facies and explosive volcanic facies. As this contact is approached VF1 and iron conglomerate IF7 facies become more common, interbedded with IF5 and IF4. In particular, outcrops of IF4 underlying VF4 were found to display syn-sedimentary microfaults (Figure 3a v). These microfaults were interpreted as synsedimentary as offset displaced individual laminations but not bedding surfaces. Outcrops of facies IF7 associated with VF1 were notable due to large subrounded clasts of bedded quartzite, and angular, laminated, hematite-rich microcrystalline chert rip ups (IF 6) reaching boulder in size, supported by a fine-grained iron grainstone-mudstone matrix (Figure 3a viii). This microcrystalline bedded chert (facies IF6), were identified as clasts rather than in place.

3.1.2. Facies Descriptions of Volcanics

Mafic massive coherent basalt flows (facies VF1; Figure 4a i) are the stratigraphically oldest volcanics in the map area. These aphanitic flows appear as resistant weathering knobs (0.5–25 m thick) in the recessive upper IF associated with facies IF4 and IF7. The other volcanics are generally more extensive and include both volcaniclastic and coherent facies, ranging in composition from mafic to felsic. Pillow basalts (VF2; Figure 4a ii) directly underlie the contact with explosive volcanism in certain locations. In most locations, this contact is marked by black basaltic-andesitic volcaniclastic breccia (VF3; Figure 4a iii, iv), which is matrix-supported with sand to cobble-sized clasts of orange-brown volcanic and altered glass fragments (Figure 4a). Overlying this, basaltic-andesitic volcaniclastic breccia (facies VF4; Figure 4a v, vi) and dacite to andesite volcaniclastic breccia (VF5; Figure 3b vii) are the most extensive facies and are generally poorly sorted, massively bedded and display features indicating subaqueous explosive eruptions such as curviplanar clasts, quenched margins and armored lapilli. The explosive facies VF4 is associated with fine-grained silty iron formation (IF5).

Overlying these explosive volcaniclastic facies are variable amygdaloidal basalt breccias (VF7; Figure 4a ix) or a volcaniclastic facies with a mafic matrix and basaltic-dacitic clasts (VF8; Figure 4a x). The clast compositions of facies VF8 appear to grade from mafic-intermediate in the west and felsic to the east.

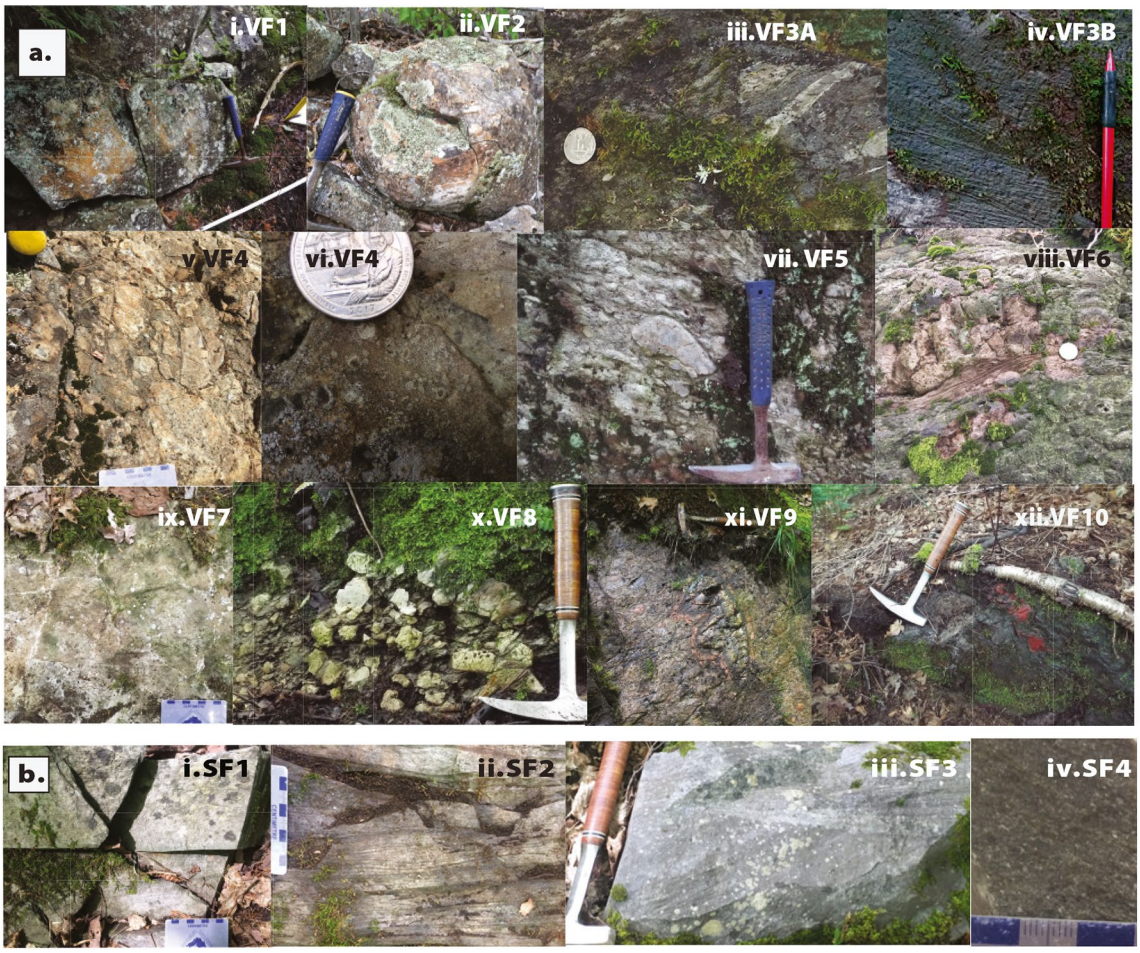

Figure 4. Field Photos continued. (a) Volcanic facies: (i) effusive basalt flow (VF1), (ii) pillow basalts (VF2) overlying IF4 and underlying VF4. (iii, iv) VF3 unit with "pseudo fiame," and cross-bedded volcaniclastic sandstone, (v, vi) curviplanar clasts and armored lapilli of VF4, (vii) intermediate-felsic VF5 with quenched margins, (viii) flow banded and bedded VF6, (ix) amygdaloidal basalt with joints VF7, (x) VF8 with resedimented felsic VF5 clasts in mafic matrix. (xi) black-green pillow breccia (VF9), (xii) VF10: black mafic flow with IF6 chert. (b) Siliciclastic facies: (i) bedded shale(SF1), (ii) flaser bedding of shale-fine sandstone interbeds (SF2), (iii) cross-bedded quartzarenite sandstone (SF3), (iv) immature siltstone (SF4).

Finally, facies VF9 and VF10 represent the stratigraphically youngest volcanics and are distinguished from the other mafic facies by their very dark green-black color combined with their dominantly coherent to autoclastic nature. Facies VF9 is a coherent-autoclastic basalt that includes pillow morphologies (Figure 4a xi), while VF10 includes aphanitic basalts, with some amygdaloidal flows and jasper clasts (Figure 4a xii).

3.1.3. Facies Descriptions of Siliciclastic Units

In the region, four siliciclastic facies were identified. These include a well-sorted tan fine mudstone (SF1; Figure 4b i) that unconformably overlies or is in fault relation with the basement. This was distinguished from SF2, a shale-siltstone-sandstone unit displaying flaser cross beds and mudstone partings with sandstone lenses (Figure 4b ii) that gradationally overlies SF1. Facies SF3 is classified as a mature sandstone with parallel and cross-bedded sedimentary structures (Figure 4b iii) that gradationally overlies SF2. Finally, facies SF4 (Figure 4b iv) is a chemically and texturally immature siltstone-sandstone that is massively bedded and unconformably overlies facies VF9, VF10, IF5, and IF2.

3.2. Depositional Interpretations

3.2.1. Interpreted Depositional Environments of the Palms Formation and Ironwood Iron Formation

The environmental interpretations (Table 1) were informed by existing work on IFs (Edwards et al., 2012; Ojakangas, 1983; Pufahl, 1996; Pufahl & Fralick, 2004) and siliciclastic frameworks (Catuneanu et al., 2009). By combining sedimentary structures and lithofacies associations with facies stacking patterns and contacts, more discerning environmental interpretations could be made.

We follow previous researchers in interpreting facies SF1-SF3 of the Palms Formation as siliciclastic transgressive sequence moving from low energy supratidal-intertidal mudflats (SF1), Low-moderate energy intertidal mud flat (SF2) to intertidal moderate to high energy tidally influenced shoreline (SF3). The basal contact between the Palms Formation and basement is not always exposed. Where it is exposed, it is erosional with clasts of Archean gneiss. In certain areas of the map area, there is no Palms Formation exposed between the IF and basement, and we interpreted this contact as a fault contact. Although it is possible that the Palms Formation was eroded or not initially deposited in these areas, there was no direct evidence in the area to motivate a change from the existing mapped relationships (Cannon et al., 2008). Both the upper Palms Formation and the lowermost observed iron facies display similar shallow-water sedimentary structures. Facies IF2 could be shelf storm deposits as suggested previously (Pufahl & Fralick, 2004), or alternatively shoreface sands. Flaser bedding is observed within facies IF1 and IF2, yet is not uniquely indicative of a specific environment or water depth, as flaser and sand-clay alternating bedding has been documented in intertidal, sub-tidal, estuarine, deltaic environments, and deeper marine environments (e.g., Baas et al., 2016; Bohacs et al., 2014; Martins et al., 2016; Quijada et al., 2016). Furthermore, the laminated iron-mudstones could be deep-water shelf deposits or tidal mudflats.

It would be best to apply sedimentologic and stratigraphic techniques to interpret the depositional cyclicity of the Ironwood Iron Formation. In IFs such as the Sokoman Iron formation in the Labrador trough and the Frere formation in Australia Pufahl (2010), Edwards et al. (2012), Akin et al. (2013), and Pufahl et al. (2014) have applied modern sequence stratigraphic techniques to clarify the IF sedimentology and stratigraphy. In such basins that have been interpreted as less affected by post-depositional processes, IF has been divided by its mineralogy into suboxic (hematite + chert) or deeper water anoxic (magnetite, greenalite, stilpnomelane) facies, and then depositional sequences are defined based on stratal stacking patterns and recognition of key bounding surfaces formed during prominent inflections during the rise and fall of sea level. Such assumptions about mineralogy reflecting primary depositional conditions would require further detailed geochemical and petrologic investigations before application to the Gogebic Range. Such past sequence stratigraphic work has provided the framework to interpret the depositional cyclicity observed in the Ironwood Iron Formation (e.g., Akin et al., 2013; Edwards et al., 2012; Pufahl, 2010; Pufahl et al., 2014). However, the outcrops examined in the present study provide equivocal paleoenvironmental interpretations, even when lithofacies associations are considered in sequence stratigraphic context.

Although the IF sequence at Wolf Mountain suffers from incomplete exposures making identification of stratal stacking patterns difficult, the facies observations and associations allow the Ironwood Iron Formation deposition to include both shallow-water and deeper-shelf environments. Though process sedimentology is conducted through analogy, Quaternary analogies are not exact comparisons to the deposits in the Gogebic Range (Chi Fru et al., 2018), and a great degree of uncertainty remains in the primary composition of IF grains (e.g., Rasmussen et al., 2021), which fundamentally links to how these grains transport and deposit. In part because of these uncertainties, we highlight the ambiguity of the depositional setting of the Gogebic Range IF facies. Even with these uncertainties, the existence of similar features preserved in the upper Palms Formation and basal Ironwood Iron Formation may question the existence of a transgressive contact. As there is no evidence for a depositional hiatus, the lithology shift may reflect changing chemistry and clastic input rather than depositional depth. This interpretation does not dramatically impact the interpretation of the upper Ironwood Iron Formation outcrops studied by Pufahl and Fralick (2004). However, it does call into question the idea that the Gogebic Range sequence is a deeper water equivalent to the Gunflint Iron Formation sequence and that both were deposited in the same contiguous basin.

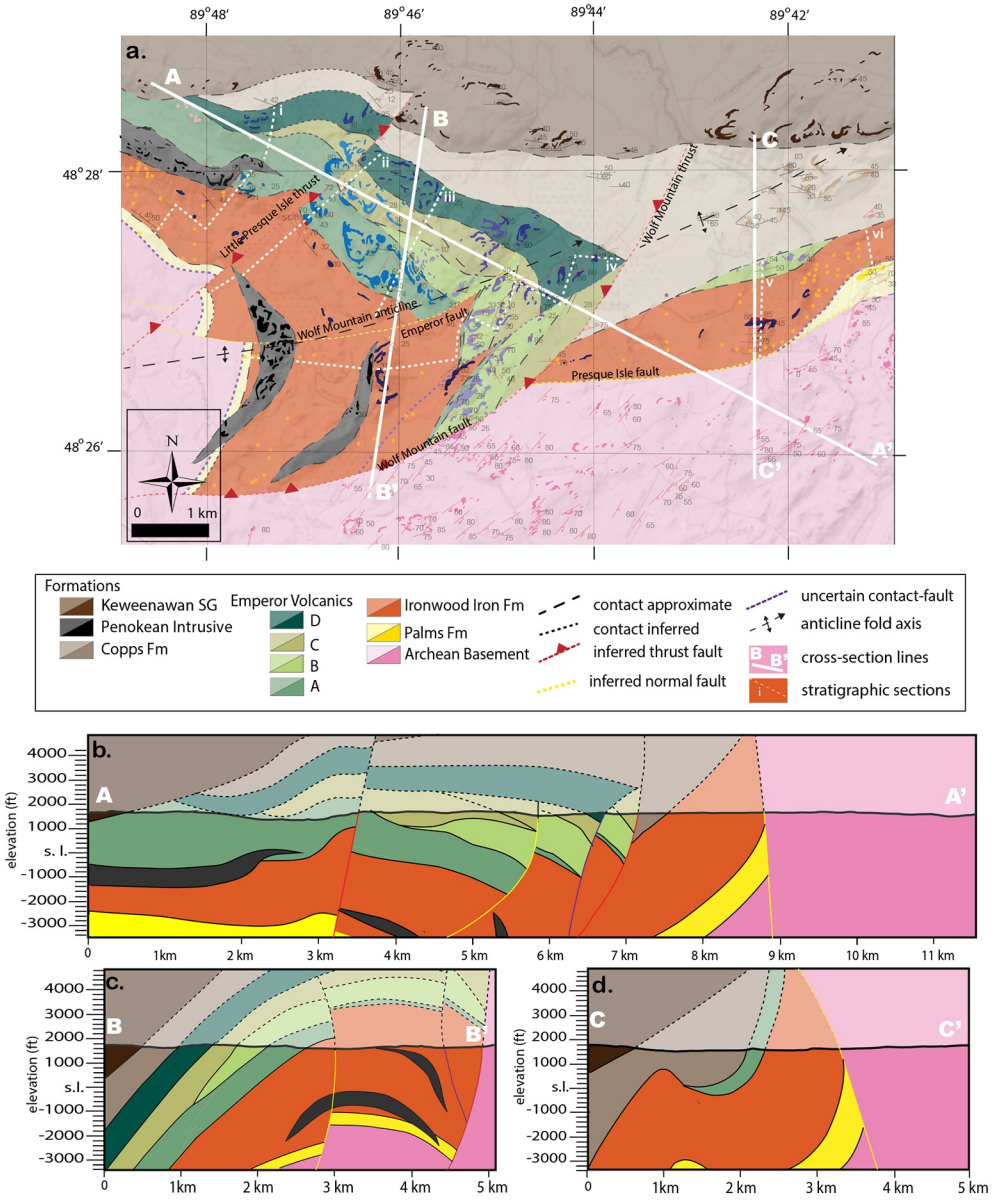

Figure 5. Wolf Mountain Interpretations. (a) Mapping interpretations with depositional and faulted contacts, overlaid by outcrop, pit and drill hole facies data (see Figure 2 for details and color key). Note the interbedded volcanic and iron formation facies (indicated by orange) in Emperor Volcanics Member A. The locations of sections used in Figure 6 are indicated (i–iv). Note, the exact thickness of iron formation in cross-sections ii and iii are not well constrained. (b–d) Wolf Mountain map cross sections. For location of Wolf Mountain area see Figure 1c. The observed thickness change in the Emperor Volcanics Member A across the yellow Emperor Fault in (A-A′ and B-B′) is interpreted as resulting from the syn-volcanic extensional activity along the normal Emperor fault.

3.2.2. Interpreted Emperor Volcanics Eruptive Sequence

The onset of Emperor Volcanics is defined as the upper contact between the often covered and recessive IF and the basal resistant outcrops of volcaniclastic facies interpreted as explosive eruptions (Figure 5). The cause for the switch from effusive to explosive volcanism itself is unclear. The main volcanic phases were grouped into Emperor Volcanics members A, B, C, and D (Figure 5a).

First, features of member A (including facies VF2-VF4), namely pillow basalts, hyaloclastites and armored lapilli are consistent with subaqueous eruptions. Although accretionary lapilli develop in air fall eruptions, armored lapilli can form with wet ash around a solid nucleus during hydrovolcanic eruptions (Cas &

Wright, 1987). Additionally, fine-grained mafic volcaniclastic units can originate in subaqueous hyaloclastite density currents (e.g., Cas & Wright, 1987).

Important for questions regarding the relationship between volcanism and IF are the mapped locations of IF5, VF3, and VF4. Iron formation facies IF5 are found in test pits in the northwestern portion of the map area (Figure 2). Although not extensive in outcrop, due to the geometry of their locations, it is likely that these test pits represent in-situ lithologies. These IF localities appear to overlie early eruptive facies VF3 and are laterally equivalent to VF4. Iron formation is interbedded both with volcanic basalt flows (VF1) within the Ironwood Iron Formation, and with the onset of the explosive volcanism of the Emperor Volcanics (member A; facies VF4). These eruptive and depositional relationships suggest that the Emperor Volcanics member A eruptions are likely coeval and time-equivalent with IF deposition.

Member B is marked by evolved intermediate to felsic compositions (facies VF5-VF6), but a similar eruptive environment to member A. In contrast, the mixed volcaniclastics of member C (facies VF8) contain clasts of members A and B, and thus represent re-deposition of members A and B within a mafic matrix. Synchronously, there is evidence for mafic volcanic autoclastic breccia being deposited as amygdaloidal flows with jigsaw fitted brecciation (facies VF7). Member C could represent reduced subaerial or subaqueous eruptions accompanied by re-mobilization of previously erupted volcanics. Finally, member D (facies VF9 and VF10) is characterized by effusive basalt flows with hematite-stained chert clasts. It could represent slightly younger volcanism, as it overlies members A–C as well as IF facies IF5. As member D basalts include pillow fragments and quenched features, they also represent subaqueous eruptions.

Despite uncertainties due to preservation bias, the absence of any volcanic outcrops stratigraphically below the IF and the increase in volcanic and tectonic influence up-section lead us to conclude that there is no direct evidence to support syn-volcanism as the trigger for the Ironwood Iron Formation deposition. Based on the current geologic data, it appears that initial volcanism postdates the onset of IF deposition. However, this dataset does not completely rule out the possibility of earlier volcanism or that volcanism elsewhere triggered iron deposition.

3.3. Structural Interpretations

The location and orientation of major faults are identified based on thickness variations between basal contacts, as well as with measured orientations of smaller, outcrop-scale, syn-sedimentary faults observed in the field. The onsets of certain eruptive facies were interpreted as marker horizons. In particular, we used (1) the onset of the explosive basaltic-andesite hyaloclastites (member A), (2) the onset of dacite-andesite hyaloclastites (member B), and (3) the onset of effusive dark basalt flows and pillows (member D). These marker horizons allowed the geometry of fault blocks in the map area to be refined and major new named faults to be identified (Figure 5a). This detailed approach has allowed new and different interpretations of regional faulting and dynamics to be clarified (Figures 5b–5d). For more details on previous interpretations, see Cannon et al., 2008; Trent, 1973 and Text S3.

To highlight these interpretations, each mapping relation is considered in turn (Figure 5), starting with the younger deformation (post-Keweenawan thrusts and Penokean compressional structures), and then considering the Paleoproterozoic structures and deformation which are particularly important for our interpretations. There are three important Keweenawan/Penokean structures, these are the Little Presque Isle thrust, and the Wolf Mountain Anticline and thrust fault. Thrust faulting along the Little Presque Isle thrust was identified based on the displacement of the Keweenawan basal contact with the Copps Formation (Figure 5). This fault activity is likely due to Grenville-aged reverse faulting (e.g., Cannon, 1994; Cannon et al., 2008). The Wolf Mountain Anticline, plunging to the northeast in its present-day geometry and impacting all the Paleoproterozoic strata, is the most obvious structural feature in the area. Although not previously recognized, we observed displacements in the basal Copps Formation-Emperor Volcanics contact, suggesting the existence of an associated Wolf Mountain thrust. This newly identified structure explains both stratigraphic differences across its east and west sides, as well as the associated generation of the Wolf Mountain Anticline.

With this more recent deformation accounted for, there are three earlier Paleoproterozoic structures with potential importance, the Emperor fault, Wolf Mountain fault, and Presque Isle fault. The mapped locations

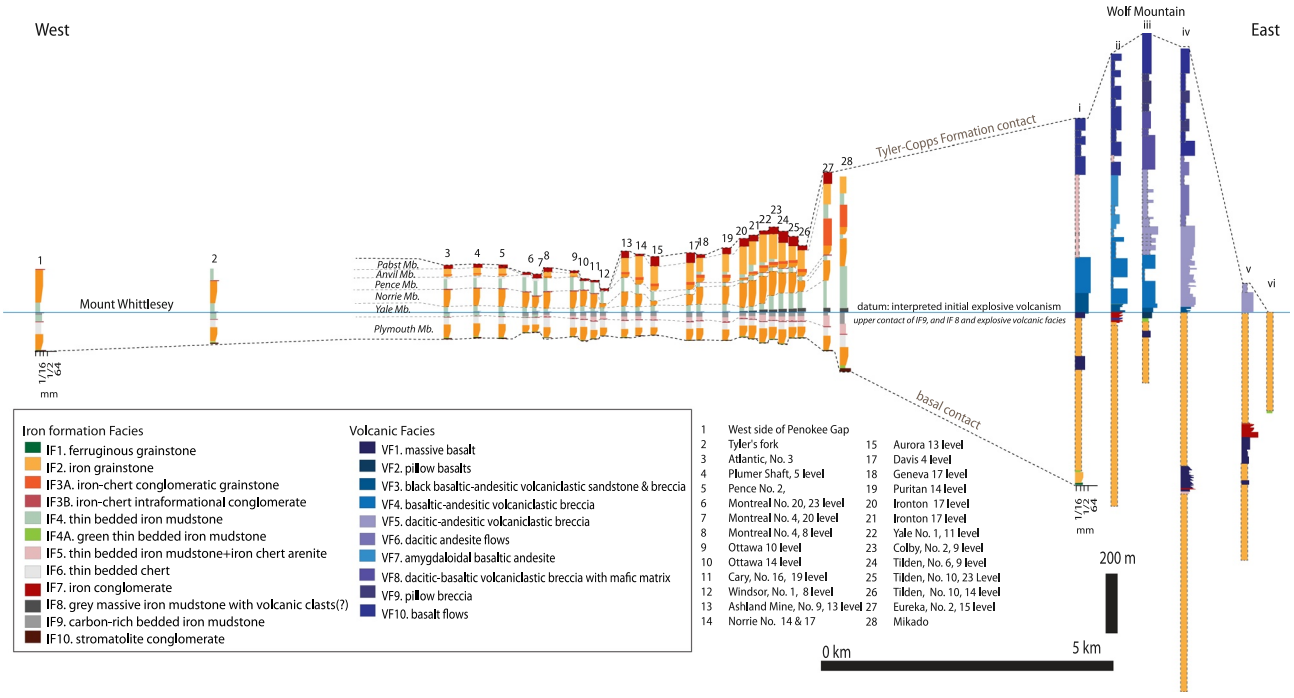

Figure 6. Stratigraphic fence diagram for the Gogebic Range, encompassing units bounded at the base by a contact with the Palms Formation and at the top by the contact with the Tyler/Copps Formation. Numbers correspond to sections and mine data (see Figure 1 and SI for locations) and roman numerals indicate sections in the Wolf mountain area, with the thickness corrected for Penokean intrusives, see Figure 5. The width of the columns represents differences in crystal/grain/clast size, with 1/16, ½, and 64 mm represented in the scale. In the Wolf Mountain area, the stratigraphic data inferred from subcrop has a dotted line around the margins.

of the onset of explosive activity (Emperor Volcanics member A) and the associated underlying IF thickness variations were used to reveal these fault locations. We propose a new fault, the Emperor fault, that is associated with the initial eruptive phases of the Emperor Volcanics. The Emperor fault is highlighted by displacements of the basal member A contact south-east on the north side. As the basal member D contact is not dramatically displaced, faulting may have ceased by the later eruptions. The IF thickness variations that existed prior to the explosive eruptions of the Emperor Volcanics suggest that the Wolf Mountain thrust may have reactivated an original normal fault, we have named the Wolf Mountain fault. Finally, we followed the existing framework regarding the basement-Paleoproterozoic strata contact as the syn-depositional Presque Isle fault (e.g., Cannon et al., 2008).

This new framework, with the Emperor fault and Wolf Mountain fault as syn-depositional, syn-eruptive listric faults related to extensional faulting along the main Presque Isle fault contrasts with previous models. Previous authors partially explained observed IF thickness variations as resulting from later fault repetition of strata due to faults parallel to bedding that were subsequently folded by the Wolf Mountain anticline (e.g., Cannon et al., 2008; Klasner et al., 1998; Prinz, 1967). This contrast with our direct observations of potential fault scarp conglomerates, syn-depositional microfaults, and facies variations that lead us to suggest that there is true stratigraphic thickening in the area related to fault activity.

4. Discussion of Results

4.1. Gogebic Range Stratigraphic Variations

By incorporating stratigraphic data from our facies mapping with data from the rest of the Gogebic Range, we find significant stratigraphic variations within the Ironwood Iron Formation (Figures 1c and 6). These thickness variations are clearly seen across the Gogebic Range stratigraphic fence diagram (Figure 6). Such fence diagrams require a datum or tie point across all the stratigraphic sections to align them. We chose as a datum the onset of explosive volcanism in the eastern portion of the Gogebic Range (VF3, VF4, or VF5),

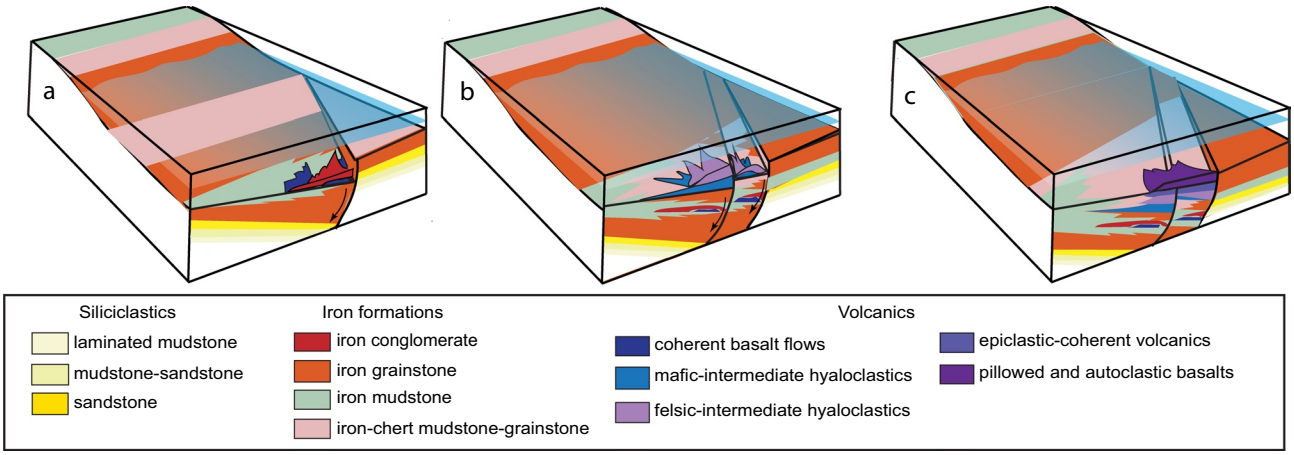

Figure 7. Model of Basin dynamics. (a) Iron formation deposition followed by onset of effusive volcanism and faulting. (b) Start of explosive hyaloclastite eruptions and continued faulting and iron formation deposition. (c) Return to effusive volcanism that may or may not postdate faulting and iron formation deposition.

the onset of IF8 deposition in the central portion (which can be interpreted as a putative volcaniclastic), and the upper contact of IF9 in the western Gogebic Range. We acknowledge uncertainties in this chosen time-correlative datum, but the main conclusions are not dramatically impacted by this choice (Figure 6).

About 200 m of stratigraphic thickness increase is seen across the Gogebic Range in the eastward approach toward Wolf Mountain stratigraphy, starting to manifest midway through the stratigraphy in units with facies IF4, IF5, IF8, and IF9 (Yale Member in the central portion of the range; see Figure 6). This is seen as mixed thin-bedded iron mudstone to iron and chert grainstone (IF5) facies that approach 113 m in thickness toward the east (approaching the Mikado mine; no. 28 in Figure 6). This thickening is accompanied by the appearance of facies IF8, a potentially distal equivalent of the Emperor Volcanics (Schmidt, 1980). Further up section, thickness variations within stratigraphic sections correlate with the appearance of coarser facies IF2, IF3 (Anvil Member). The thickness of the uppermost iron grainstone facies dominated by IF2 increases abruptly eastward from the Windsor Mine (no. 12 in Figure 6) to the Ashland mine (no. 13 in Figure 5) and continues to increase eastward toward the Eureka Mine (no. 27 in Figure 6).

Analysis of this compilation and associated fence diagram, suggests that thickness variations start at or below the base of the Yale Member. This is consistent with some of the suggestions by Hotchkiss (1919) and Schmidt (1980). Furthermore, we posit that the thickness variations reflect fault-influenced sedimentation in the Gogebic basin by the time of Yale Member deposition. This onset of active sedimentation explains why Schmidt (1980) had such difficulty in matching his general Yale Member observations (mostly from the central-eastern part of the Gogebic Range) with the Yale Member details from Hotchkiss (1919) which was primarily based on work in the western Gogebic Range.

4.2. Gogebic Range Basin Dynamics

The basin dynamics are highlighted through the identified facies relationships within the Emperor Volcanics in the Wolf Mountain locality. The location and orientation of major syn-sedimentary faults were identified based on thickness variations of the IF underlying the explosive volcanic facies across the map area, as well as with measured orientations of smaller, outcrop-scale, syn-sedimentary faults observed in the field. Based on our results, we propose the following model for Gogebic Range basin dynamics during IF deposition (Figure 7). After IF deposition commenced, the eastern Gogebic Range experienced faulting and effusive basaltic magmatism (Figure 7a i). This faulting continued, while the magmatism changed from mafic to intermediate, explosive hyaloclastites, followed by intermediate–to-felsic hyaloclastites (Figure 7a ii). During faulting and explosive subaqueous eruptions, IF deposition continued across the Gogebic Range with significant lateral facies variability, as evidenced by coarse fault-scarp conglomerates, and juxtapositions of iron mudstone and iron grainstone dominated units. Subsequently, there was a change in volcanism

to effusive amygdaloidal flows accompanied by remobilization and reworking of the previously erupted volcanics. Finally, sedimentation via re-mobilization was followed by a return to effusive basaltic magmatism that could have postdated the IF deposition and faulting in the area (Figure 7a iii). Broadly, variations in sedimentology, facies and stratigraphy suggest that much of the Gogebic Range IF was deposited in an active extensional tectonic setting. However, based on the fence diagram (Figure 5) we emphasize that thickness appears to increase to the east partway through the stratigraphy. Although it may be possible that thickening encompasses the entire IF stratigraphy, our correlation suggests that thickening was initiated partway through the deposition, and not at the base of the entire section. These observations include the basal IF facies, the later relative onset of effusive volcanism and fault-related sedimentation, and the similarity in the basal iron facies at Wolf Mountain and farther west in the Gogebic Range.

4.3. Implications for Models of Transgressive Shelf Sedimentation of Massive Iron Deposits

Given this integrated stratigraphic dataset from across the Gogebic Range, we document and highlight stratigraphic thickening linked to facies changes in coarse conglomerates and inferred syn-sedimentary faults. We interpret these thickness variations to be tectonically mediated and suggest that the onset of Ironwood Iron Formation may not be consistent with transgressive continental margin shelf deposition. Although regional geologists have already adopted more active tectonic frameworks for the IFs of the Superior region (e.g., Fralick et al., 2002; 2017; Hoffman, 1987; Schneider et al., 2002), transgressive continental margin shelf environments (aka. "transgressive passive margins") are still discussed in recent literature for "Superior" style and ~1.88 Ga IFs (Cawood & Hawkesworth, 2015; Craddock, et al., 2018; Egglseder, et al., 2017; Groves & Santosh, 2020; Hiatt et al., 2015; Konhauser et al., 2017; Lechte & Wallace, 2015; Pietrzak-Renaud & Davis, 2014; Pufahl et al., 2014; Raye et al., 2015; Rodrigues et al., 2019; Schröder & Warke, 2016). Regardless of the choice of exact tectonic setting, be it localized tectonics, extensional tectonism across the Superior Craton or accretionary tectonics related the amalgamation of Laurentia (e.g., Heaman et al., 2009; Whitmeyer & Karlstrom, 2007), here evidence is presented that highlights the dynamic nature of Superior style IFs and supports the conclusion that massive IFs across the GOE span a diversity of tectonic settings.

4.4. Global Context for the Post-GOE Iron Formation Depositional Trigger

The driving question for this work is, what conditions triggered the development of the largest pulse in IF since the initial rise of atmospheric oxygen? There are several possible mechanisms: (a) continental margin shelf transgressions, (b) intense volcanism and (c) a shifting chemocline due to fluctuating atmospheric oxygen, ocean chemistry, or pH. In these models, IF deposits are generally predicted at the chemocline between oxic surface waters and basinal ferruginous waters (Simonson & Hassler, 1996), or on deeper water shelves during storms due to the mixing of oxic water with ferruginous water masses (Pufahl & Fralick, 2004).

The dataset presented here from the Gogebic Range contradicts the transgressive model for IF initially proposed by Ojakangas (1983), where global transgressions allow greater water depths and enhanced iron deposition across continental margins. Specifically, our facies relationships illustrate the active nature of the Gogebic basin sedimentation and our IF facies with current-generated sedimentary structures highlight the possibility that iron deposition occurred in both deep and shallow environments (Figure 7). We suggest that transgressions and regressions still play a role in sedimentation style as suggested for some exposures of the upper stratigraphy in the western Gogebic Range (Pufahl & Fralick, 2004). However, our model suggests that transgressions and regressions were not the primary controls on IF deposition. Instead, tectonism played a more primary role in the distribution of facies across the Gogebic Range than previously considered.

The facies identified in the Gogebic Range are similar to IF facies identified in the Frere, Sokoman and Biwabik Iron Formations as detailed by previous authors (Akin et al., 2013; Edwards et al., 2012; Pufahl, 1996; Pufahl, 2010; Pufahl et al., 2014). Although the tectonic context for IFs in the Lake Superior Region included stable shelf interpretations in the past (Ojakangas, 1983; Simonson & Hassler, 1996), active margin models have more recently been proposed (e.g., Fralick et al., 2002, 2017; Hoffman, 1987; Schneider et al., 2002). Stable continental ("passive") margin interpretations seem less controversial for potentially

time-correlative IF in the Labrador trough (Edwards et al., 2012; Pufahl, 2010; Pufahl & Hiatt, 2012; Pufahl et al., 2014) and in the Australian Nabberu basin (Akin et al., 2013). In both of these basins sequence stratigraphic data has been used to show that the IF deposits form entirely on a stable shelf environment. However, even in those cases, the transgressive model falls apart as sequence stratigraphic work has highlighted evidence for shallow peritidal IF deposition, showing that the onset of deposition cannot simply be related to marine transgression (Akin et al., 2013; Edwards et al., 2012; Pufahl et al., 2014; Pufahl & Hiatt, 2012).

Rather than the transgressive continental shelf margin model for IF deposition, an external trigger for IF deposition may need to be invoked. As detailed earlier, the co-occurrence of similarly aged intrusive and extrusive volcanics around the Superior craton has led many to suggest that intense volcanism triggered the onset of IF (Bekker et al., 2014; Isley & Abbott, 1999; Konhauser et al., 2017). However, our field relationships suggest that volcanism occurred after IF deposition started, and so a syn-basinal volcanic trigger for the Ironwood Iron Formation should not be considered. Furthermore, as the Emperor Volcanics are included in the Circum-Superior Magmatic Province, our data suggest that the link between that ~1.88 Ga large igneous province and iron deposition may not be as strong as hitherto thought. Instead, if indeed volcanism is paramount for triggering post-GOE iron deposition, it would need to be distally sourced, potentially from a different large igneous province event, large-scale extensional or accretionary magmatism related to supercontinent dynamics, or enhanced mid-ocean ridge spreading. There are underexplored impacts of a proposed ~1.99 Ga Large Igneous Province (LIP) that could have influenced ocean iron concentrations and led to the onset of ~1.88 Ga iron deposition (Ernst et al., 2021; Kastek et al., 2018). However, given the time delay between the proposed ~1.99 Ga LIP and proposed ~1.88 Ga onset of iron deposition, the 1.99 LIP volcanism alone is less probable as a direct trigger for iron deposition. Our Gogebic Range observations of the non-causal relationship between syn-basinal volcanism and iron deposition question the hypothesis that volcanic pulses trigger IFs and prompt reexamination of the relationships between IFs and possible volcanic influences in other basins.

This new data from the Gogebic Range appears similar to the evaluation of other IF basins. Although volcanically influenced sedimentation occurs mid-section in the Gunflint Iron Formation, there appears to be minimal impact of volcaniclastic material on iron-formation deposition (Fralick et al., 2002; Hassler & Simonson, 1989). Farther south in the assumed correlative Mesabi Range Biwabik Iron Formation, volcanic influence at a similar stratigraphic height has been suggested, but not definitively identified. In Michigan, closer to Marquette, IF may interfinger with the bimodal Hemlock volcanics (Schneider et al., 2002); however, map relations also allow the possibility that volcanics may in fact overlie the IF (Cannon & Klasner, 1976; Gair & Wier, 1956). Considering the data presented in this study, other IFs around Lake Superior may have been deposited in similar settings to the Gogebic Range.

Farther north in the Labrador Trough, arc volcanics overlie IF, and at certain localities additional volcanics may be coeval with iron deposition (e.g., Findlay et al., 1995; Machado et al., 1988). Yet, more pristine localities of Sokoman Iron Formation have been geochemically examined to suggest that localized volcanic activity is not a prerequisite for IF accumulation (Raye et al., 2015). The least deformed Sokoman Iron Formation samples exhibit LREE enrichment and slight positive Eu anomalies or negative Eu anomalies, consistent with a weak to limited hydrothermal signature or siliciclastic contamination (Raye et al., 2015). Furthermore, the detailed stratigraphy and sedimentology of basins not associated with volcanics, such as the Australian Frere Formation, led Akin et al. (2013) to argue that IF deposition does not necessitate a volcanic prelude. These studies seem to corroborate our results, signifying that although IF deposition may have a hydrothermal Fe source and co-occur with volcanics, extensive and intense volcanism might not be the trigger for the onset of IF deposition. It may also be possible that hydrothermal activity influenced chemistry prior to the onset of volcanism, but that would need to be tested by detailed geochemical and petrological analyses and the work conducted by this study did not identify any outcrop or thin section observations that required invoking any earlier hydrothermal alteration or activity.

When considering the results of this study within the global context, we suggest that IFs were not confined to continental margin shelf transgressions, or even a specific tectonic setting, but were deposited over a much larger range of environments and settings. This is consistent with early work by Trendall (1968) who suggested that broad depositional basins may have existed, but certain localities may have been complicated by troughs and lagoons, and also consistent with Morey and Southwick (1995) who advocated that IFs were

deposited during progressive growth and ultimate destruction of a rifted continental margin. Thus, not only is post-GOE IF deposition not likely triggered by marine transgressions alone, but also iron deposition might include basin restriction and tectonic deepening, which may complicate interpretations for global ocean conditions.

Along with the observed textural variabilities between pre-GOE and post-GOE IFs, there may be important distinctions between the locus and drivers of IF deposition across such a key atmospheric change. While the transgressive shelf model may explain the deeper shelf onset of some of the pre-GOE IFs, it is not consistent with the pulse of younger post-GOE IFs. Furthermore, future research should refrain from considering these deposits together as a uniform "Superior iron formations" classification and should instead evaluate pre- and post-GOE continental margin IFs separately.

We have focused this work on understanding physical rather than chemical controls on IF deposition after the initial rise of atmospheric oxygen. However, by ruling out both syn-basinal volcanism and transgression as necessary for IF initiation, we suggest that fluctuating global atmospheric oxygen or aqueous O_2 or pH may have triggered this post-GOE pulse. This buttresses atmospheric oxygen or basin chemistry focused hypotheses for the onsets of other IF occurrences (Beukes & Gutzmer, 2008; Edwards et al., 2012; Fralick et al., 2017; Halevy et al., 2017; Johnson et al., 2018; Pufahl, 2010; Rasmussen et al., 2016; Tosca et al., 2016). The mechanisms for such a shift in global atmospheric O_2 could involve perturbations in the fluxes of reductants to space, reductants into the mantle, reductants from the deep Earth, or biological O_2 production (e.g., Catling et al., 2001; Claire et al., 2006; Zahnle et al., 2013). Instead of atmospheric O_2 shifts, the chemocline itself could be shifted due to fluctuating surface water O_2 levels linked to phytoplankton population dynamics or strong sub-seafloor hydrothermal circulation of anoxic waters (Edwards et al., 2012; Fralick et al., 2017; Pufahl, 2010). Perturbations in ocean pH or chemistry could be achieved by changes in the rate and composition of weathered materials (i.e., continental weathering of sulfides) or the CO_2 concentration in the ocean, which is mediated by temperature or atmospheric CO_2 (e.g., Bekker & Holland, 2012; Krissansen-Totton et al., 2018). Resultant increases in pH could trigger the precipitation of iron, as has been proposed for Neoarchean and older Paleoproterozoic pre-GOE IFs (Beukes & Gutzmer, 2008; Johnson et al., 2018; Rasmussen et al., 2015, 2017). It is suggested that Fe^{2+} could precipitate via biotic and abiotic pathways as iron silicates or green rust (Crowe et al., 2008; Halevy et al., 2017; Johnson et al., 2018; Kappler & Newman, 2004; Tosca et al., 2016; Zegeye et al., 2007, 2012). While global conditions may regulate iron deposition, it is possible that the basinal chemical conditions for iron deposition may be enhanced by the tectonic regime. This may especially be true for restricted basins or expanded shallow-water environments. New geochemical and petrographic work within a detailed stratigraphic context such as presented here is needed to decipher between these mechanisms and elucidate Proterozoic environments that emerged after the initial rise of oxygen.

5. Conclusions

Here we have combined new stratigraphic and mapping relationships with mine data and logs to refine the basin model for the Ironwood Iron Formation and Emperor Volcanics. Our new Wolf Mountain thrust explains the development of the Penokean Wolf Mountain anticline. Identification of the new Emperor fault provides a framework to understand stratigraphic thickening. Importantly, bedding parallel faults are not necessary to explain the thickness changes at Wolf Mountain, and the thickness increase is part of a general thickening trend across the Gogebic Range tied to syn-sedimentary faulting within the basin. Thus, the Gogebic Range Ironwood Iron Formation deposition is not consistent with a transgressive continental shelf sequence. This point is significant as a transgressive model cannot be applied to the basin and instead IF onset requires an external trigger. Although not the first to discuss the possibility of a tectonically dynamic environment, we are the first to present a dataset to quantify and link the westward thickening with tectonic activity during IF deposition.

Our dataset also suggests that the initiation of significant syn-basinal volcanism, linked to a large igneous province, does not coincide with the onset of Ironwood Iron Formation deposition. Thus, intense syn-basinal volcanism cannot be invoked as a trigger for IF deposition. Furthermore, as the onset of faulting may have post-dated the onset of IF, a particular regional tectonic setting may not have triggered the IF pulse.

Iron formation deposition may be consistent with chemocline shallowing due to changes in atmospheric oxygen.

Data Availability Statement

Data and data products related to the paper are available via the Dryad data repository: https://doi.org/10.5061/dryad.1g1jwsts1.

Acknowledgments
We thank the Bergmann group for early comments and C. Condit and D. Ojakangas for helpful discussions. This manuscript benefited from insightful and detailed reviews from Peir Pufahl, Philip Fralick, and an anonymous reviewer. We also appreciate the professional and comprehensive editorial handling by Josh Feinberg. Financial support for this research was provided by the MIT EAPS W. O. Crosby Postdoctoral Fellowship and the Johns Hopkins EPS Morton K. Blaustein Postdoctoral Fellowship to A. Eyster and the Packard Foundation to K. Bergmann. There are no real or perceived financial conflicts of interests for any of the authors.

References

Addison, W. D., Brumpton, G. R., Vallini, D. A., McNaughton, N. J., Davis, D. W., Kissin, S. A., et al. (2005). Discovery of distal ejecta from the 1850 Ma Sudbury impact event. *Geology*, *33*(3), 193–196. https://doi.org/10.1130/g21048.1

Akin, S. J., Pufahl, P. K., Hiatt, E. E., & Pirajno, F. (2013). Oxygenation of shallow marine environments and chemical sedimentation in Palaeoproterozoic peritidal settings: Frere Formation, Western Australia. *Sedimentology*, *60*(7), 1559–1582. https://doi.org/10.1111/sed.12038

Aldrich, H. R. (1929). The geology of the Gogebic iron range of Wisconsin: Wisc. *Geological and Natural History Survey: Economic Series Bulletin*.

Allen, R. C., & Barrett, L. P. (1915). *A revision of the sequence and structure of the pre-Keweenawan formations of the eastern Gogebic iron range* (Vol. 18, pp. 33–83). Michigan Geological and Biological Survey Publication.

Baas, J. H., Best, J. L., & Peakall, J. (2016). Predicting bedforms and primary current stratification in cohesive mixtures of mud and sand. *Journal of the Geological Society*, *173*(1), 12–45. https://doi.org/10.1144/jgs2015-024

Barley, M. E., Bekker, A., & Krapež, B. (2005). Late Archean to Early Paleoproterozoic global tectonics, environmental change and the rise of atmospheric oxygen. *Earth and Planetary Science Letters*, *238*(1–2), 156–171. https://doi.org/10.1016/j.epsl.2005.06.062

Bekker, A., & Holland, H. D. (2012). Oxygen overshoot and recovery during the early Paleoproterozoic. *Earth and Planetary Science Letters*, *317*, 295–304. https://doi.org/10.1016/j.epsl.2011.12.012

Bekker, A., Planavsky, N., Rasmussen, B., Krapez, B., Hofmann, A., Slack, J., et al. (2014). Iron formations: Their origins and implications for ancient seawater chemistry. *Treatise on geochemistry*, *12*, 561–628. https://doi.org/10.1016/b978-0-08-095975-7.00719-1

Bekker, A., Slack, J. F., Planavsky, N., Krapez, B., Hofmann, A., Konhauser, K. O., & Rouxel, O. J. (2010). Iron formation: The sedimentary product of a complex interplay among mantle, tectonic, oceanic, and biospheric processes. *Economic Geology*, *105*(3), 467–508. https://doi.org/10.2113/gsecongeo.105.3.467

Beukes, N. J. (1983). Palaeoenvironmental setting of iron-formations in the depositional basin of the Transvaal Supergroup, South Africa. *Developments in Precambrian Geology*, *6*, 131–198. https://doi.org/10.1016/s0166-2635(08)70043-4

Beukes, N. J., & Gutzmer, J. E. N. S. (2008). Origin and paleoenvironmental significance of major iron formations at the Archean-Paleoproterozoic boundary. *Reviews in Economic Geology*, *15*, 5–47. https://doi.org/10.5382/rev.15.01

Bleeker, W. (2003). The late Archean record: A puzzle in ca. 35 pieces. *Lithos*, *71*(2–4), 99–134. https://doi.org/10.1016/j.lithos.2003.07.003

Bleeker, W., & Kamo, S. L. (2017). Extent, origin, and deposit-scale controls of the 1883 Ma circum-superior large igneous province, northern Manitoba, Ontario, Quebec, Nunavut and Labrador. In *Targeted geoscience initiative* (pp. 5–14).

Bohacs, K. M., Lazar, O. R., & Demko, T. M. (2014). Parasequence types in shelfal mudstone strata—Quantitative observations of lithofacies and stacking patterns, and conceptual link to modern depositional regimes. *Geology*, *42*(2), 131–134. https://doi.org/10.1130/g35089.1

Bunting, J. A. (1986). Geology of the eastern part of the Nabberu Basin Western Australia. *Geological Survey of Western Australia Bulletin*, *131*, 130.

Cannon, W. F. (1994). Closing of the Midcontinent rift-A far—Field effect of Grenvillian compression. *Geology*, *22*(2), 155–158. https://doi.org/10.1130/0091-7613(1994)022<0155:cotmra>2.3.co;2

Cannon, W. F., & Klasner, J. S. (1976). *Geological map and geophysical interpretation of the Witch Lake Quadrangle, Marquette, Iron, and Baraga counties (No. 987)*.

Cannon, W. F., LaBerge, G. L., Klasner, J. S., & Schulz, K. J. (2008). The Gogebic Iron Range—A sample of the northern margin of the Penokean fold and thrust belt (No. 1730). *US Geological Survey*.

Cas, R. A. F., & Wright, J. V. (1987). *Volcanic successions: Modern and ancient*. Allen and Unwin.

Catling, D. C., Zahnle, K. J., & McKay, C. P. (2001). Biogenic methane, hydrogen escape, and the irreversible oxidation of early Earth. *Science*, *293*(5531), 839–843. https://doi.org/10.1126/science.1061976

Catuneanu, O., Abreu, V., Bhattacharya, J. P., Blum, M. D., Dalrymple, R. W., Eriksson, P. G., et al. (2009). Towards the standardization of sequence stratigraphy. *Earth-Science Reviews*, *92*(1–2), 1–33. https://doi.org/10.1016/j.earscirev.2008.10.003

Cawood, P. A., & Hawkesworth, C. J. (2015). Temporal relations between mineral deposits and global tectonic cycles. *Geological Society, London, Special Publications*, *393*(1), 9–21. https://doi.org/10.1144/sp393.1

Chi Fru, E., Kilias, S., Ivarsson, M., Rattray, J. E., Gkika, K., McDonald, I., et al. (2018). Sedimentary mechanisms of a modern banded iron formation on Milos Island, Greece. *Solid Earth*, *8*. https://doi.org/10.5194/se-9-573-2018

Ciborowski, T. J. R., Minifie, M. J., Kerr, A. C., Ernst, R. E., Baragar, B., & Millar, I. L. (2017). A mantle plume origin for the Palaeoproterozoic Circum-Superior large Igneous Province. *Precambrian Research*, *294*, 189–213. https://doi.org/10.1016/j.precamres.2017.03.001

Claire, M. W., Catling, D. C., & Zahnle, K. J. (2006). Biogeochemical modelling of the rise in atmospheric oxygen. *Geobiology*, *4*(4), 239–269. https://doi.org/10.1111/j.1472-4669.2006.00084.x

Conliffe, J. (2015). Geological setting and genesis of high-grade iron ore deposits in the Eastern Labrador Trough. *Newfoundland and Labrador Department of Natural Resources Geological Survey Report*, *15*, 1–25.

Craddock, J. P., Malone, D. H., Schmitz, M. D., & Gifford, J. N. (2018). Strain variations across the Proterozoic Penokean orogen, USA and Canada. *Precambrian Research*, *318*, 25–69. https://doi.org/10.1016/j.precamres.2018.09.004

Crowe, S. A., Jones, C., Katsev, S., Magen, C., O'Neill, A. H., Sturm, A., et al. (2008). Photoferrotrophs thrive in an Archean Ocean analogue. *Proceedings of the National Academy of Sciences*, *105*(41), 15938–15943. https://doi.org/10.1073/pnas.0805313105

Dann, J. C. (1978). *Major-element variation within the emperor igneous complex and the Hemlock and Badwater volcanic formations*. Michigan Technological University.

Davis, D. W., & Paces, J. B. (1990). Time resolution of geologic events on the Keweenaw Peninsula and implications for development of the Midcontinent Rift system. *Earth and Planetary Science Letters*, *97*(1–2), 54–64. https://doi.org/10.1016/0012-821x(90)90098-i

Derry, L. A., & Jacobsen, S. B. (1990). The chemical evolution of Precambrian seawater: Evidence from REEs in banded iron formations. *Geochimica et Cosmochimica Acta*, *54*(11), 2965–2977. https://doi.org/10.1016/0016-7037(90)90114-z

Edwards, C. T., Pufahl, P. K., Hiatt, E. E., & Kyser, T. K. (2012). Paleoenvironmental and taphonomic controls on the occurrence of Paleoproterozoic microbial communities in the 1.88 Ga Ferriman Group, Labrador Trough, Canada. *Precambrian Research*, *212*, 91–106. https://doi.org/10.1016/j.precamres.2012.04.020

Egglseder, M. S., Cruden, A. R., Dalstra, H. J., & Nicholas, L. (2017). The role of deformation in the formation of banded iron formation-hosted high-grade iron ore deposits, Hamersley Province (Australia). *Precambrian Research*, *296*, 62–77. https://doi.org/10.1016/j.precamres.2017.04.034

Ernst, R. E., & Bell, K. (2010). Large igneous provinces (LIPs) and carbonatites. *Mineralogy and Petrology*, *98*(1–4), 55–76. https://doi.org/10.1007/s00710-009-0074-1

Ernst, R. E., Bond, D. P., Zhang, S. H., Buchan, K. L., Grasby, S. E., Youbi, N., et al. (2021). *Large igneous province record through time and implications for secular environmental changes and geological time-scale BoundariesLarge igneous provinces: A driver of global environmental and biotic changes* (pp. 1–26). https://doi.org/10.1002/9781119507444.ch1

Evans, D. A. D., Li, Z. X., & Murphy, J. B. (2016). Four-dimensional context of Earth's supercontinents. *Geological Society, London, Special Publications*, *424*(1), 1–14. https://doi.org/10.1144/sp424.12

Evans, D. A. D., & Mitchell, R. N. (2011). Assembly and breakup of the core of Paleoproterozoic–Mesoproterozoic supercontinent Nuna. *Geology*, *39*(5), 443–446. https://doi.org/10.1130/g31654.1

Findlay, J. M., Parrish, R. R., Birkett, T. C., & Watanabe, D. H. (1995). U–Pb ages from the Nimish Formation and Montagnais glomeroporphyritic gabbro of the central New Québec Orogen, Canada. *Canadian Journal of Earth Sciences*, *32*(8), 1208–1220. https://doi.org/10.1139/e95-099

Fischer, W. W., & Knoll, A. H. (2009). An iron shuttle for deepwater silica in Late Archean and early Paleoproterozoic iron formation. *The Geological Society of America Bulletin*, *121*(1–2), 222–235.

Floran, R. J., & Papike, J. J. (1975). Petrology of the low-grade rocks of the Gunflint Iron-Formation, Ontario-Minnesota. *The Geological Society of America Bulletin*, *86*(9), 1169–1190. https://doi.org/10.1130/0016-7606(1975)86<1169:potlro>2.0.co;2

Fralick, P., & Barrett, T. J. (1995). Depositional controls on iron formation in Canada. In *Sedimentary Facies Analysis* (Vol. 22, pp. 137–156). International Association of Sedimentologists, Spec Pub.

Fralick, P., Davis, D. W., & Kissin, S. A. (2002). The age of the Gunflint Formation, Ontario, Canada: Single zircon U-Pb age determinations from reworked volcanic ash. *Canadian Journal of Earth Sciences*, *39*(7), 1085–1091. https://doi.org/10.1139/e02-028

Fralick, P., Planavsky, N., Burton, J., Jarvis, I., Addison, W. D., Barrett, T. J., & Brumpton, G. R. (2017). Geochemistry of Paleoproterozoic Gunflint formation carbonate: Implications for hydrosphere-atmosphere evolution. *Precambrian Research*, *290*, 126–146. https://doi.org/10.1016/j.precamres.2016.12.014

French, B. M. (1968). Progressive contact metamorphism of the Biwabik Iron formation, Mesabi Range, Minnesota. *Minnesota Geological Survey*, *45*, 103.

French, B. M. (1973). Mineral assemblages in diagenetic and low- grade metamorphic iron-formation. *Economic Geology*, *68*, 1063–1074. https://doi.org/10.2113/gsecongeo.68.7.1063

Gair, J. E., & Wier, K. L. (1956). *Geology of the Kiernan quad. Iron Co*. U.S. Geological Survey.

Gole, M. J., & Klein, C. (1981). Banded iron-formations through much of Precambrian time. *The Journal of Geology*, *89*(2), 169–183. https://doi.org/10.1086/628578

Goode, A. D. T., Hall, W. D. M., & Bunting, J. A. (1983). The Nabberu Basin of Western Australia. *Developments in Precambrian Geology*, *6*, 295–323. https://doi.org/10.1016/s0166-2635(08)70046-x

Gross, G. A. (1983). Tectonic systems and the deposition of iron-formation. *Developments in Precambrian Geology*, *7*, 63–79. https://doi.org/10.1016/s0166-2635(08)70242-1

Gross, G. A., & Zajac, I. S. (1983). Iron-formation in fold belts marginal to the Ungava craton. *Developments in Precambrian Geology*, *6*, 253–294. https://doi.org/10.1016/s0166-2635(08)70045-8

Groves, D. I., & Santosh, M. (2020). Craton and thick lithosphere margins: The sites of giant mineral deposits and mineral provinces. *Gondwana Research*. https://doi.org/10.1016/j.gr.2020.06.008

Halevy, I., Alesker, M., Schuster, E. M., Popovitz-Biro, R., & Feldman, Y. (2017). A key role for green rust in the Precambrian oceans and the genesis of iron formations. *Nature Geoscience*, *10*(2), 135–139. https://doi.org/10.1038/ngeo2878

Hall, W. D. M., & Goode, A. D. T. (1978). The early Proterozoic Nabberu Basin and associated iron formations of Western Australia. *Precambrian Research*, *7*(2), 129–184. https://doi.org/10.1016/0301-9268(78)90031-1

Hassler, S. W., & Simonson, B. M. (1989). Deposition and alteration of volcaniclastic strata in two large, early Proterozoic iron-formations in Canada. *Canadian Journal of Earth Sciences*, *26*(8), 1574–1585. https://doi.org/10.1139/e89-134

Heaman, L. M., Peck, D., & Toope, K. (2009). Timing and geochemistry of 1.88 Ga Molson Igneous Events, Manitoba: Insights into the formation of a craton-scale magmatic and metallogenic province. *Precambrian Research*, *172*(1–2), 143–162. https://doi.org/10.1016/j.precamres.2009.03.015

Hemming, S. R., McLennan, S. M., & Hanson, G. N. (1995). Geochemical and Nd/Pb isotopic evidence for the provenance of the Early Proterozoic Virginia Formation, MN: Implications for the tectonic setting of the Animikie Basin. *The Journal of Geology*, *103*, 147–168. https://doi.org/10.1086/629733

Hiatt, E. E., Pufahl, P. K., & Edwards, C. T. (2015). Sedimentary phosphate and associated fossil bacteria in a Paleoproterozoic tidal flat in the 1.85 Ga Michigamme Formation. *Sedimentary Geology*, *319*, 24–39. https://doi.org/10.1016/j.sedgeo.2015.01.006

Hoffman, P. F. (1987). Early Proterozoic foredeeps, foredeep magmatism, and superior-type iron-formations of the Canadian Shield. *Proterozoic Lithospheric Evolution*, *17*, 85–98. https://doi.org/10.1029/gd017p0085

Hoffman, P. F. (1988). United plates of America, the birth of a craton: Early Proterozoic assembly and growth of Laurentia. *Annual Review of Earth and Planetary Sciences*, *16*(1), 543–603. https://doi.org/10.1146/annurev.ea.16.050188.002551

Hotchkiss (1919). Geology of the Gogebic range and its relation to recent mining developments. *Engineering and Mining Journal*, *108*, 443–452.

Huber, N. K. (1959). Some aspects of the origin of the Ironwood iron-formation of Michigan and Wisconsin. *Economic Geology*, *54*(1), 82–118. https://doi.org/10.2113/gsecongeo.54.1.82

Huston, D. L., & Logan, G. A. (2004). Barite, BIFs and bugs: Evidence for the evolution of the Earth's early hydrosphere. *Earth and Planetary Science Letters*, *220*(1–2), 41–55. https://doi.org/10.1016/s0012-821x(04)00034-2

Irving, R. D., & Van Hise, C. R. (1892). *Penokean Iron Bearing Series of Michigan and Wisconsin*. (Monograph 19) (p. 534). USGS.
Isley, A. E., & Abbott, D. H. (1999). Plume-related mafic volcanism and the deposition of banded iron formation. *Journal of Geophysical Research*, *104*(B7), 15461–15477. https://doi.org/10.1029/1999jb900066
James, H. L. (1954). Sedimentary facies of iron-formation. *Economic Geology*, *49*(3), 235–293. https://doi.org/10.2113/gsecongeo.49.3.235
James, H. L. (1955). Zones of regional metamorphism in the Precambrian of northern Michigan. *The Geological Society of America Bulletin*, *66*, 1455–1488. https://doi.org/10.1130/0016-7606(1955)66[1455:zormit]2.0.co;2
Johnson, J. E., & Molnar, P. H. (2019). Widespread and persistent deposition of iron formations for two billion years. *Geophysical Research Letters*, *46*, 3327–3339. https://doi.org/10.1029/2019GL081970
Johnson, J. E., Muhling, J. R., Cosmidis, J., Rasmussen, B., & Templeton, A. S. (2018). Low-Fe (III) Greenalite was a primary mineral from Neoarchean Oceans. *Geophysical Research Letters*, *45*(7), 3182–3192. https://doi.org/10.1002/2017gl076311
Kappler, A., & Newman, D. K. (2004). Formation of Fe (III)-minerals by Fe (II)-oxidizing photoautotrophic bacteria. *Geochimica et Cosmochimica Acta*, *68*(6), 1217–1226. https://doi.org/10.1016/j.gca.2003.09.006
Kastek, N., Ernst, R. E., Cousens, B. L., Kamo, S. L., Bleeker, W., Söderlund, U., et al. (2018). U-Pb Geochronology and geochemistry of the Povungnituk Group of the Cape Smith Belt: Part of a craton-scale circa 2.0 Ga Minto-Povungnituk large igneous province, northern Superior craton. *Lithos*, *320*, 315–331. https://doi.org/10.1016/j.lithos.2018.09.026
Kimberley, M. M. (1989). Exhalative origins of iron formations. *Ore Geology Reviews*, *5*(1–2), 13–145. https://doi.org/10.1016/0169-1368(89)90003-6
Klasner, J. S., LaBerge, G. I., & Cannon, W. F. (1998). *Geologic map of the eastern Gogebic iron range, Gogebic County, Michigan* (pp. I–2606). USGS.
Klasner, J. S., Ojakangas, R. W., Schulz, K. J., & LaBerge, G. L. (1991). Nature and style of deformation in the foreland of the Early Proterozoic Penokean orogen, northern MI. *U.S. Geological Survey Bulletin*.
Klein, C. (1966). Mineralogy and petrology of the metamorphosed Wabush Iron Formation, southwestern Labrador. *Journal of Petrology*, *7*(2), 246–305. https://doi.org/10.1093/petrology/7.2.246
Klein, C. (1973). Changes in mineral assemblages with metamorphism of some banded Precambrian iron-formations. *Economic Geology*, *68*(7), 1075–1088. https://doi.org/10.2113/gsecongeo.68.7.1075
Klein, C. (1978). Regional metamorphism of Proterozoic iron-formation, Labrador Trough, Canada. *American Mineralogist*, *63*(9–10), 898–912.
Klein, C. (1983). Diagenesis and metamorphism of Precambrian banded iron-formations. *Developments in Precambrian Geology*, *6*, 417–469. https://doi.org/10.1016/s0166-2635(08)70052-5
Klein, C. (2005). Some Precambrian banded iron-formations (BIFs) from around the world: Their age, geologic setting, mineralogy, metamorphism, geochemistry, and origins. *American Mineralogist*, *90*(10), 1473–1499. https://doi.org/10.2138/am.2005.1871
Klein, C., & Beukes, N. J. (1992a). Proterozoic iron-formations. *Developments in Precambrian Geology*, *10*, 383–418. https://doi.org/10.1016/s0166-2635(08)70124-5
Klein, C., & Beukes, N. J. (1992b). Time distribution, stratigraphy, and sedimentologic setting, and geochemistry of Precambrian iron-formations. In J. W. Schopf, & C. Klein (Eds.), *The Proterozoic biosphere: A multidisciplinary study* (pp. 139–147). Cambridge University Press.
Klein, C., & Fink, R. P. (1976). Petrology of the Sokoman Iron Formation in the Howells River area, at the western edge of the Labrador Trough. *Economic Geology*, *71*(2), 453–487. https://doi.org/10.2113/gsecongeo.71.2.453
Knoll, A. H., & Beukes, N. J. (2009). Introduction: Initial investigations of a Neoarchean shelf margin-basin transition (Transvaal Supergroup, South Africa). *Precambrian Research*, *169*(1–4), 1–14. https://doi.org/10.1016/j.precamres.2008.10.009
Konhauser, K. O., Planavsky, N. J., Hardisty, D. S., Robbins, L. J., Warchola, T. J., Haugaard, R., et al. (2017). Iron formations: A global record of Neoarchaean to Palaeoproterozoic environmental history. *Earth-Science Reviews*, *172*, 140–177. https://doi.org/10.1016/j.earscirev.2017.06.012
Krissansen-Totton, J., Arney, G. N., & Catling, D. C. (2018). Constraining the climate and ocean pH of the early Earth with a geological carbon cycle model. *Proceedings of the National Academy of Sciences*, *115*(16), 4105–4110. https://doi.org/10.1073/pnas.1721296115
LaBerge, G. L. (1964). Development of magnetite in iron formations of the Lake Superior region. *Economic Geology*, *59*(7), 1313–1342. https://doi.org/10.2113/gsecongeo.59.7.1313
Laybourn, D. P. (1979). *The geology and metamorphism of the Ironwood iron-formation, Gogebic range, Wisconsin*. (Doctoral dissertation). University of Minnesota.
Lechte, M. A., & Wallace, M. W. (2015). Sedimentary and tectonic history of the Holowilena Ironstone, a Neoproterozoic iron formation in South Australia. *Sedimentary Geology*, *329*, 211–224. https://doi.org/10.1016/j.sedgeo.2015.09.014
Lepp, H. (1987). Chemistry and origin of Precambrian iron-formations. In P. W. U. Appel, & G. L. LaBerge (Eds.), *Precambrian iron-formations: Athens, Greece* (pp. 3–30). Theophrastus Publications.
Lyons, T. W., Reinhard, C. T., & Planavsky, N. J. (2014). The rise of oxygen in Earth's early ocean and atmosphere. *Nature*, *506*(7488), 307–315. https://doi.org/10.1038/nature13068
Machado, N., Perreault, S., & Hynes, A. (1988). Timing of continental collision in the northern Labrador Trough: Evidence from U - Pb geochronology. *Geological Association of Canada-Mineralogical Association of Canada, Program and Abstracts*, *13*, A76.
Martins, S. E., Barcellos, R. L., Flores-Montes, M. J., & de França, E. J. (2016). Depositional evolution in a estuarine lagoonal system under a port influence in Northeastern Brazil. *Journal of Coastal Research*, *75*, 84–88. https://doi.org/10.2112/si75-017.1
McPhie, J., Doyle, M., & Allen, R. (1993). *Volcanic textures: A guide to the interpretation of textures in volcanic rocks* (p. 1993). Centre for Ore Deposit and Exploration Studies, University of Tasmania.
Mengel, J. T. (1973). Physical sedimentation in Precambrian cherty iron formations of the Lake Superior type. In *Ores in sediments* (pp. 179–193). Springer. https://doi.org/10.1007/978-3-642-65329-2_14
Minifie, M. J., Kerr, A. C., Ernst, R. E., Hastie, A. R., Ciborowski, T. J. R., Desharnais, G., & Millar, I. L. (2013). The northern and southern sections of the western ca. 1880 Ma circum-Superior large igneous province, North America: The Pickle Crow dyke connection? *Lithos*, *174*, 217–235. https://doi.org/10.1016/j.lithos.2012.03.017
Morey, G. B. (1969). *SP-07 the geology of the middle Precambrian Rove formation in northeastern Minnesota Minnesota geological survey*. University of Minnesota Digital Conservancy. Retrieved from https://hdl.handle.net/11299/59958
Morey, G. B., & Southwick, D. L. (1995). Allostratigraphic relationships of Early Proterozoic Iron-formations in the Lake Superior region. *Economic Geology*, *90*(7), 1983–1993. https://doi.org/10.2113/gsecongeo.90.7.1983
Morris, R. C., & Horwitz, R. C. (1983). The origin of the iron-formation-rich Hamersley Group of Western Australia—Deposition on a platform. *Precambrian Research*, *21*(3–4), 273–297. https://doi.org/10.1016/0301-9268(83)90044-x

Ojakangas, R. W. (1983). Tidal deposits in the early Proterozoic basin of the Lake Superior region. In *The early Proterozoic geology of the Great Lakes region* (Vol. 160, p. 49). https://doi.org/10.1130/mem160-p49

Ojakangas, R. W., Morey, G. B., & Southwick, D. L. (2001). Paleoproterozoic basin development and sedimentation in the Lake Superior region, North America. *Sedimentary Geology*, *141–142*, 319–341. https://doi.org/10.1016/s0037-0738(01)00081-1

Pietrzak-Renaud, N., & Davis, D. (2014). U–Pb geochronology of baddeleyite from the Belleview metadiabase: Age and geotectonic implications for the Negaunee Iron Formation. *Precambrian Research*, *250*, 1–5. https://doi.org/10.1016/j.precamres.2014.05.018

Poulton, S. W., Fralick, P. W., & Canfield, D. E. (2010). Spatial variability in oceanic redox structure 1.8 billion years ago. *Nature Geoscience*, *3*(7), 486–490. https://doi.org/10.1038/ngeo889

Prinz, W. C. (1967). *Pre-Quaternary geologic and magnetic map and sections of part of the eastern Gogebic Iron Range*. (Miscellaneous geologic investigations 1) (p. 497). US Geol. Survey.

Prinz, W. C. (1981). *Geologic map of the Gogebic range-Watersmeet area, Gogebic and Ontonagon Counties*. (No. 1365).

Pufahl, P. K. (1996). *Stratigraphic architecture of a Paleoproterozoic iron formation depositional system: The Gunflint, Mesabi and Cuyuna iron ranges* (Msc. Thesis).

Pufahl, P. K. (2010). Bioelemental sediments. In N. P. James, & R. W. Dalrymple (Eds.), *Facies models* (4th ed., pp. 477–504). Geological Association of Canada.

Pufahl, P. K., Anderson, S. L., & Hiatt, E. E. (2014). Dynamic sedimentation of Paleoproterozoic continental margin iron formation, Labrador Trough, Canada: Paleoenvironments and sequence stratigraphy. *Sedimentary Geology*, *309*, 48–65. https://doi.org/10.1016/j.sedgeo.2014.05.006

Pufahl, P. K., & Fralick, P. W. (2000). Geology of the Paleoproterozoic Gunflint Formation. In *Institute on Lake Superior Geology, Proceedings, Part 2* (Vol. 46). Fieldtrip Guide Book.

Pufahl, P. K., & Fralick, P. W. (2004). Depositional controls on Palaeoproterozoic iron formation accumulation, Gogebic range, Lake Superior region, USA. *Sedimentology*, *51*(4), 791–808. https://doi.org/10.1111/j.1365-3091.2004.00651.x

Pufahl, P. K., & Hiatt, E. E. (2012). Oxygenation of the Earth's atmosphere–ocean system: A review of physical and chemical sedimentologic responses. *Marine and Petroleum*.

Quijada, I. E., Suarez-Gonzalez, P. A. B. L. O., Benito, M. I. & Mas, R. (2016). Tidal versus continental sandy-muddy flat deposits: Evidence from the Oncala Group (Early Cretaceous, N Spain). In *Contributions to modern and ancient tidal sedimentology: Proceedings of the tidalites 2012 Conference* (pp. 133–159). https://doi.org/10.1002/9781119218395.ch8

Rasmussen, B., Fletcher, I. R., Bekker, A., Muhling, J. R., Gregory, C. J., & Thorne, A. M. (2012). Deposition of 1.88-billion-year-old iron formations as a consequence of rapid crustal growth. *Nature*, *484*(7395), 498–501. https://doi.org/10.1038/nature11021

Rasmussen, B., Krapež, B., Muhling, J. R., & Suvorova, A. (2015). Precipitation of iron silicate nanoparticles in early Precambrian oceans marks Earth's first Iron Age. *Geology*, *43*(4), 303–306. https://doi.org/10.1130/g36309.1

Rasmussen, B., Muhling, J. R., & Fischer, W. W. (2019). Evidence from laminated chert in banded iron formations for deposition by gravitational settling of iron-silicate muds. *Geology*, *47*(2), 167–170. https://doi.org/10.1130/g45560.1

Rasmussen, B., Muhling, J. R., & Krapež, B. (2021). Greenalite and its role in the genesis of early Precambrian iron formations–A review. *Earth-Science Reviews*, *217*, 103613. https://doi.org/10.1016/j.earscirev.2021.103613

Rasmussen, B., Muhling, J. R., Suvorova, A., & Krapež, B. (2016). Dust to dust: Evidence for the formation of "primary" hematite dust in banded iron formations via oxidation of iron silicate nanoparticles. *Precambrian Research*, *284*, 49–63. https://doi.org/10.1016/j.precamres.2016.07.003

Rasmussen, B., Muhling, J. R., Suvorova, A., & Krapež, B. (2017). Greenalite precipitation linked to the deposition of banded iron formations downslope from a late Archean carbonate platform. *Precambrian Research*, *290*, 49–62. https://doi.org/10.1016/j.precamres.2016.12.005

Raye, U., Pufahl, P. K., Kyser, T. K., Ricard, E., & Hiatt, E. E. (2015). The role of sedimentology, oceanography, and alteration on the δ56Fe value of the Sokoman Iron Formation, Labrador Trough, Canada. *Geochimica et Cosmochimica Acta*, *164*, 205–220.

Reed, R. C., & Daniels, J. (1987). *Bedrock geology of northern MichiganGeological survey division. 1:500,000 scale*. Michigan Department of Natural Resources.

Robbins, L. J., Funk, S. P., Flynn, S. L., Warchola, T. J., Li, Z., Lalonde, S. V., et al. (2019). Hydrogeological constraints on the formation of Palaeoproterozoic banded iron formations. *Nature Geoscience*, *12*, 558–563.

Rodrigues, P. D. O. C., Hinnov, L. A., & Franco, D. R. (2019). A new appraisal of depositional cyclicity in the Neoarchean-Paleoproterozoic Dales Gorge Member (Brockman Iron Formation, Hamersley Basin, Australia). *Precambrian Research*, *328*, 27–47.

Schmidt, R. G. (1980). *The Marquette range Supergroup in the Gogebic iron district, Michigan and Wisconsin; B; 1460*. U.S. Govt. Print. Off.

Schneider, D. A., Bickford, M. E., Cannon, W. F., Schulz, K. J., & Hamilton, M. A. (2002). Age of volcanic rocks and syndepositional iron formations, Marquette Range Supergroup: Implications for the tectonic setting of Paleoproterozoic iron formations of the Lake Superior region. *Canadian Journal of Earth Sciences*, *39*(6), 999–1012.

Schröder, S., & Warke, M. R. (2016). Termination of BIF deposition in the Paleoproterozoic: The Tongwane Formation, South Africa. *South African Journal of Geology*, *119*(2), 329–346.

Schulz, K. J., & Cannon, W. F. (2007). The Penokean orogeny in the Lake Superior region. *Precambrian Research*, *157*, 4–25.

Simonson, B. M. (1985). Sedimentological constraints on the origins of Precambrian iron-formations. The *Geological Society of America Bulletin*, *96*(2), 244–252.

Simonson, B. M. (2003). Origin and evolution of large Precambrian iron formations. In M. A. Chan, & A. W. Archer (Eds.), *Extreme depositional environments: Mega end members in geologic time* (pp. 231–244). Geological Society of America Special Paper 370. https://doi.org/10.1130/0-8137-2370-1.231

Simonson, B. M., & Hassler, S. W. (1996). Was the deposition of large Precambrian iron formations linked to major marine transgressions? *The Journal of Geology*, *104*(6), 665–676.

Sims, P. K. (1992). *Geological map of Precambrian rocks, southern Lake Superior region, Wisconsin and northern Michigan*. (USGS_I-2185). USGS.

Sims, P. K., Peterman, Z. E., Prinz, W. C., & Benedict, F. C. (1984). *Geology, geochemistry, and age of Archean and Early Proterozoic rocks in the Marinesco-Watersmeet area, northern Michigan*. (Paper, 1292-A, A1–A41). US Geol. Surv. Prof.

Sims, P. K., Schmus, W. V., Schulz, K. J., & Peterman, Z. E. (1989). Tectono-stratigraphic evolution of the Early Proterozoic Wisconsin magmatic terranes of the Penokean Orogen. *Canadian Journal of Earth Sciences*, *26*(10), 2145–2158.

Southwick, D. L., & Morey, G. B. (1991). Tectonic imbrication and fore- deep development of the Penokean orogen, east-central Minne- sota Ð an interpretation based on regional geophysics and the results of test-drilling. *US Geological Survey Bulletin*, *17*, 1904.

Tosca, N. J., Guggenheim, S., & Pufahl, P. K. (2016). An authigenic origin for Precambrian greenalite: Implications for iron formation and the chemistry of ancient seawater. *GSA Bulletin*, *128*(3–4), 511–530.

Trendall, A. F. (1968). Three great basins of Precambrian banded iron formation deposition: A systematic comparison. *The Geological Society of America Bulletin*, *79*(11), 1527–1544.
Trendall, A. F. (2002). The significance of iron-formation in the Precambrian stratigraphic record. In. *Precambrian sedimentary environments: A modern approach to ancient depositional systems* (pp. 33–66).
Trent, V. A. (1973). *Geologic map of the Marenisco and Wakefield NE quadrangles Gogebic County*. (No. 73-280).
Van Hise, C. R., & Leith, C. K. (1911). *The geology of the Lake Superior region (No. 52)*. US Government Printing Office.
Van Wyck, N., & Johnson, C. (1997). Common Pb, Sm–Nd, and U–Pb constraints on the petrogenesis, crustal architecture, and tectonic setting of the Penokean orogen (Paleoproterozoic) in Wisconsin. *The Geological Society of America Bulletin*, *109*, 799–808.
Whitmeyer, S. J., & Karlstrom, K. E. (2007). Tectonic model for the Proterozoic growth of North America. *Geosphere*, *3*(4), 220–259.
Zahnle, K. J., Catling, D. C., & Claire, M. W. (2013). The rise of oxygen and the hydrogen hourglass. *Chemical Geology*, *362*, 26–34.
Zajac, I. S. (1974). The stratigraphy and mineralogy of the Sokoman Formation in the Knob Lane Area, Quebec and Newfoundland. *Geological Survey of Canada Bulletin*, *220*, 159.
Zegeye, A., Bonneville, S., Benning, L. G., Sturm, A., Fowle, D. A., Jones, C., et al. (2012). Green rust formation controls nutrient availability in a ferruginous water column. *Geology*, *40*(7), 599–602.
Zegeye, A., Ruby, C., & Jorand, F. (2007). Kinetic and thermodynamic analysis during dissimilatory γ-FeOOH reduction: Formation of green rust 1 and magnetite. *Geomicrobiology Journal*, *24*(1), 51–64.
Zi, J. W., Sheppard, S., Muhling, J. R., & Rasmussen, B. (2021). Refining the Paleoproterozoic tectonothermal history of the Penokean Orogen: New U-Pb age constraints from the Pembine-Wausau terrane, Wisconsin, USA. *GSA Bulletin*.